

Go-or-Grow Models in Biology: a Monster on a Leash

Ryan Thiessen^{a,‡}, Martina Conte^{*,b,‡}, Tracy L. Stepien^c, and Thomas Hillen^a

^a *Department of Mathematical and Statistical Sciences, University of Alberta, Edmonton, Canada*

^b *Department of Mathematical, Physical, and Computer Sciences, University of Parma, Italy*

^c *Department of Mathematics, University of Florida, Gainesville, FL, USA*

February 24, 2026

Abstract

Go-or-grow approaches represent a specific class of mathematical models used to describe populations where individuals either migrate or reproduce, but not both simultaneously. These models have a wide range of applications in biology and medicine, chiefly among those the modeling of brain cancer spread. The analysis of go-or-grow models has inspired new mathematics, and it is the purpose of this review to highlight interesting and challenging mathematical properties of reaction–diffusion models of the go-or-grow type. We provide a detailed review of biological and medical applications before focusing on key results concerning solution existence and uniqueness, pattern formation, critical domain size problems, and traveling waves. We present new general results related to the critical domain size and traveling wave problems, and we connect these findings to the existing literature. Moreover, we demonstrate the high level of instability inherent in go-or-grow models. We argue that there is currently no accurate numerical solver for these models, and emphasize that special care must be taken when dealing with the “monster on a leash”.

Keywords – Go-or-grow dichotomy | Glioma | Traveling Waves | Instabilities and Patterns | Critical domain size

MSC codes – 92B05, 35B36, 35M30

1 Introduction

Various biological processes involve a dichotomy between proliferation and migration: individuals in a population either remain relatively stationary and reproduce, or they migrate with minimal reproduction. This phenomenon has been particularly emphasized in the study of glioma progression, where the “go-or-grow” hypothesis was coined to describe the behavior of brain tumor cells [48].

The seminal work by Murray et al. [88] laid the groundwork for much of the existing mathematical modeling of glioma spread, which is based on the classical Fisher–Kolmogorov–Petrovsky–Piskounov (FKPP) equation. This reaction–diffusion macroscopic mathematical

*Corresponding author: conte.martina.93@gmail.com

‡These authors contributed equally to the work.

framework has been termed as the proliferation–infiltration (PI) model, as it captures both the proliferative and invasive behaviors of glioma cells observed in experiments and clinical settings. The strength of the PI model lies in its simplicity, requiring only a small set of parameters, which facilitates its calibration to patient-specific data. Extensions of the PI model account for the influence of surrounding tissue, chemical signals, and/or vasculature on glioma cell density [20, 25, 26, 53, 62, 103, 114–116]. Advection bias in response to environmental cues has also been incorporated, either directly in the macroscopic model, based on mass/flux/momentum balance [18, 65], or through more detailed descriptions derived from lower-scale dynamics, as initially proposed in [93] and further developed in [19, 21, 22, 31–33, 113]. Many models have also been developed in (semi)discrete settings [7, 48, 66]. However, due to the complexity of glioma growth—spanning interactions between glioma cells, their microenvironment, immune cells, vasculature, and molecular signalling systems, all within the heterogeneous landscape of brain tissue—an exhaustive model remains elusive. As a result, models typically focus on well-defined subprocesses. Among these, the phenotypic heterogeneity of glioma cells plays a central role. While there are numerous reviews of mathematical modeling of gliomas [1, 49, 64, 84], this paper specifically focuses on a family of reaction–diffusion models of the go-or-grow type. In these models, a distinct separation between proliferating and migrating cells leads to systems of two coupled reaction–diffusion equations.

We will focus our attention on a minimal go-or-grow model consisting of two coupled differential equations for the evolution of a moving subpopulation and a resting and proliferating subpopulation of cells. We assume linear diffusion for the moving population and neglect any small diffusivity in the resting population. Concerning the transition functions between the two subpopulations, we account for a general dependence on both subpopulation densities, defining this setting as the *general go-or-grow model*. As described above, there are several extensions of this framework that may include nonlinear diffusion of the moving compartment, general waiting time distributions, small diffusivity in the stationary compartment, or more complex population dynamics. Their analysis is rich, well-developed, and their analytical properties are vast [9, 37, 67, 88, 108].

1.1 Paper outline

We first provide in Section 2 a detailed overview of the use of go-or-grow models for describing glioma dynamics (Section 2.1), reviewing the biological evidence of the go-or-grow dichotomy in glioma (Section 2.1.1) and the mathematical literature of go-or-grow models formulated with discrete, continuous, deterministic and stochastic approaches (Section 2.2). We also discuss applications of the go-or-grow dichotomy in ecology and other biological settings (Section 2.3).

In Section 3, we first review the classical FKPP equation as a reference point for further modeling and analysis. We then introduce the main players of this review article, namely the *general go-or-grow model* and its simplifications, which we call the *total population go-or-grow model*, where the transition functions depend on the sum of the two subpopulation densities [8, 34, 48, 97, 111, 117, 121], and the *balanced go-or-grow model* and *constant rates go-or-grow model*, which fit into the context analyzed in [8, 34, 37, 41, 42, 97, 117]. We show that for fast transition rates, a FKPP-type model can be found as the leading order approximation.

After the models are defined, we focus on some mathematical properties. In Section 4, we review a method by Rothe [101] to obtain a general local and global existence result. This does, however, not prevent strange behavior, as we show in Section 5. Here we employ methods that

were developed by Marciniak-Czochra et al. [47, 82], to find that high-frequency instabilities are possible, and in fact, likely to occur. Section 6 focuses on the classical ecological problem of a critical domain size, investigating what is the minimum size of a domain to support a go-or-grow population by reviewing previous results of Hadeler et al. [46, 74]. Section 7 then focuses on the existence of invasion waves and the estimation of the invasion speeds. We review previous results by Hadeler et al. [46], Pham et al. [97], Stepien et al. [111], and Falcó et al. [34], and put them into an extended general framework. For this, we employ the general theory of invasion fronts of cooperative systems to generate a new result that applies in our more general framework. This section closes with a comparison of the wave speeds of the go-or-grow models to the FKPP wave speed.

This paper is rounded off with a discussion (Section 8) of the relevance of these models to both biology and mathematics and the mathematical challenges that are still open. The biological applications are manifold, and the mathematical problems are interesting and challenging.

2 Biological background and previous mathematical models

2.1 Motivation: glioma dynamics

Gliomas are the most frequent type of primary brain tumors. They originate from glial cells in the central nervous system and account for 78% percent of malignant brain tumors, of which glioblastoma multiforme (GBM) is the most aggressive subtype. It is characterized by infiltrative spread and fast proliferation. These features make GBMs relentless and deadly brain cancers, claiming the lives of most patients within eighteen months of diagnosis, with only a small percentage surviving beyond five years [91, 129].

A significant challenge stems from the highly invasive nature of gliomas, characterized by diffuse borders and recurrence of the disease around or within the treated area [54]. Glioma cells not only invade locally, navigating through the extracellular matrix (ECM), but also exploit structured pathways such as myelinated fibers, vasculature, and white matter tracts, enabling them to travel great distances [24, 31, 53, 90, 103, 113]. This results in GBMs often presenting with a heterogeneous and anisotropic shape.

2.1.1 Biological evidence of go-or-grow dichotomy in glioma

Many experiments with cultures of glioma cells suggest mutual exclusion of migratory and proliferative behavior, a mechanism known as the go-or-grow dichotomy [5, 36, 43–45, 126, 130], schematized in Figure 1. Precisely, in [43, 44] experimental evidence suggests that there may be an inherent and inverse correlation between cell motility and proliferation within a malignant glioma cell population, i.e., highly migratory glioma cells have a lower proliferation rate compared to those cells with weak migratory ability that proliferate much more. In [45], a glioma-expressed microRNA that regulates the balance of proliferation and migration in response to metabolic stress is identified, revealing that, in addition to inhibiting glioma cell migration, this microRNA expression also promotes cell proliferation. The role of the receptor tyrosine kinase EphB2 in controlling the proliferation/migration dichotomy in GBMs and its pro-invasive and anti-proliferative effects is later shown in [126]. In [52], the go-or-grow behavior is also observed in melanoma cells, although other studies suggest that the behavior appears to be specific to tumors of glial origin [40].

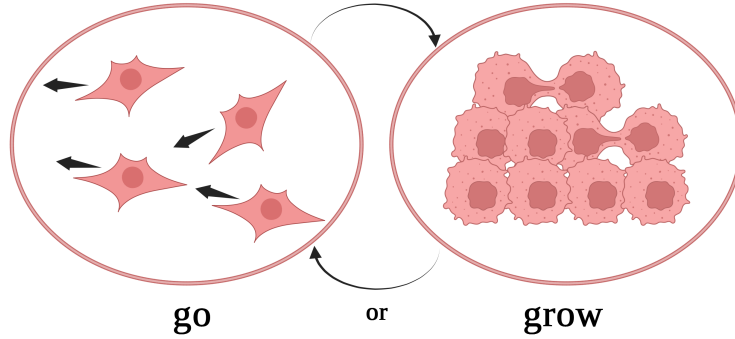


Figure 1: **Sketch of the go-or grow dichotomy.** In this framework, cells can switch between a moving phenotype and a stationary and reproducing phenotype. Created in BioRender. Conte, M. (2024) <https://BioRender.com/i82o612>

However, the go-or-grow hypothesis does not apply to all tumor growth in general. For example, in [89, 99] the authors identified glioblastoma cells that exhibit both high proliferative and invasive capabilities simultaneously. In [4, 104], the emergence of a go-and-grow phenotype under hypoxic conditions is observed. Similarly, in [124] it is shown for melanoma that differentiating between solely moving or proliferating cancer cells could not be determined. Hence, the go-or-grow mechanism is not a universal phenomenon in cancer, although it has been reported in many cases and most prominently in glioma.

2.2 Mathematical approaches to the go-or-grow dichotomy in glioma

The large literature concerning mathematical models for the description of the go-or-grow mechanism in gliomas ranges from (semi)discrete to continuous approaches, from hybrid to stochastic methods. Moreover, within models of the same family, further classifications can be considered in relation to either the type of considered phenotypic switch functions (e.g. constant, density-dependent rates, or environmental-driven switching) or the characteristic of the operators modeling migration (e.g. linear or nonlinear diffusion, as well as additional tactic terms).

2.2.1 Stochastic and discrete models

One of the first publications investigating the go-or-grow mechanism is the model by Fedotov and Iomin [37, 38] that uses a continuous time random walk (CTRW) to formulate the balance equations for the cancer cells of two phenotypes with random switching between cell proliferation and migration. The CTRW describes tumor cell transport, assuming an arbitrary waiting time distribution between jumps and general jump kernels, while proliferation is modeled by a logistic growth. The authors study the overall spreading rate, defined as the speed of the traveling wave solution of their system, and find its dependence on the statistical characteristics of the random switching process. From these first works, the literature on this topic started to expand.

A series of papers from Hatzikirou, Deutsch, and co-authors analyze the problem using lattice-gas cellular automaton (LGCA) models that account for unbiased cell random walk and cell proliferation influenced by the local oxygen concentration and according to a carrying capacity-limited mechanism. Phenotype changes either with constant probabilities [7, 48],

local cell density-dependent rates [8, 117, 118], or in response to environmental stimuli [66]. The width of the invasive zone and the speed of the invasive front are analyzed in relation to the phenotypic transition parameter. In particular, in [8, 117] the authors distinguish two scenarios depending on the parameter regions. In one case, called repulsive regime, the tumor cell population will inevitably grow. In the other case, called attractive regime, they identified conditions under which sufficiently small tumors die out. This is a phenomenon known as the Allee effect and it is deeply studied in ecology. Mean field approximations of the LGCA models are also provided, under the assumption that the switch dynamics are much faster than cell proliferation and death. The authors derive macroscopic descriptions of FKPP type, showing that there is a trade-off between diffusion and proliferation, reflecting the inability of cells to migrate and proliferate simultaneously.

With a methodology similar to [37], in [41, 42] Gerlee and Nelander develop an individual-based (IB) stochastic model with constant switching rates between proliferating or migrating states. From it, they derive a system of macroscopic PDEs that establishes a connection between single cell characteristics and macroscopic behaviors. Precisely, their strategy is to formulate two coupled master equations for the occupation probabilities of the lattice sites and then approximate them by a set of PDEs. The derived macroscopic system features nonlinear diffusion for both cell populations, as well as additional transport for the moving cells, which makes the model different from the our minimal go-or-growth setting. Wave speed analysis is performed to show the influence of the parameters (switching, proliferation, motility, and apoptosis rate) on the wave speed. Moreover, under suitable simplified assumptions, a closed expression of the minimum wave speed is derived, as well as an approximate expression of the wavefront shape, using singular perturbation methods.

2.2.2 Continuous models

Inspired by the macroscopic counterparts of the above-described discrete approaches modeling the go-or-growth dichotomy in glioma cells, continuous formulations of such mechanism have been proposed. These approaches are either derived from multi-scale descriptions of cell dynamics or directly stated at the macroscopic level as reaction–diffusion models.

Concerning multi-scale models, the first setting is described in [13], where the authors build a model for two interacting cell populations with different migratory properties whose corresponding phenotype changes are induced by cell density effects. In particular, they investigate the phenotypic adaptation to dense and sparse environments, showing that when the cell migratory ability is reduced by a crowded environment, a diffusive instability may appear, leading to the formation of aggregates of cells of the same phenotype. Similar approaches to the same problem have been later proposed in a series of works accounting for the go-or-grow cell mechanism in response to constant or density-dependent rates [3, 33, 51, 137] as well as different environmental factor, such as oxygen and nutrient availability, acidity [22], therapy effects [61], or cell membrane receptors’ concentration [112]. These approaches feature non-linear diffusion and transport terms for the moving cells. Moreover, in some of these works, results concerning the global existence of weak solutions for the derived macroscopic setting are proved [112, 137]. In this category, we also have to mention a recent work from Hillen and co-authors [51], who propose a mathematical model for the microtubule-induced glioma invasion in which, under suitable scaling arguments, a go-or-grow mechanism could be identified, *a posteriori*, justifying the earlier approaches. The idea of microtubule-mediated cell invasion comes from some recent experiments [90] showing how glioma cells send out thin cell protrusions - the tumor microtubules - that form a network invading the healthy tissue, making

connections between cells and enabling long-range cell-to-cell signaling. 198

Considering models directly stated at the macroscopic level in terms of reaction–diffusion 199
systems of equations for the two cell sub-populations, a first approach can be found in [97]. 200
The described setting models a density-dependent go-or-grow mechanism, characterizing the 201
development of spatio-temporal instabilities and traveling wave solutions. In the same context 202
of density-dependent phenotypic changes, we must also account for the investigations collected 203
in [34, 111, 121]. Precisely, in [111] the authors analyze the speed and shape of traveling wave 204
solutions of a go-or-grow model for some specific expression of the phenotypic transition 205
functions. They derive a closed form for the minimum wave speed and, adapting the method 206
of Canosa [11], obtain an approximation of the traveling wave solution. This study has been 207
then extended in [121] for slightly more general phenotypic transition functions. Recently, in 208
[34], a formal analysis of the traveling wave solutions has been presented in comparison with 209
the classical results of the well-known FKPP equation. However, this has been obtained with 210
simplified assumptions on the transition parameters, comparable with considering constant 211
rate functions. Besides these studies, which relate to a minimal go-or-grow model similar to 212
(4), it is worthy to mention some other works developed within the same biological context 213
that, however, either account for small diffusion terms in the equation for the proliferative 214
population [10, 94] or consider phenotypic transition rates depending on external signals [2, 215
4, 23, 83, 103, 109, 110]. Models that incorporate the microenvironment include [23] where 216
the authors analyze a heterogeneous population comprising cells that can either move and 217
degrade ECM or proliferate, including both nonlinear diffusion and an additional tactic term 218
for the former, as well as the evolution of the ECM. They explore the impact of different 219
switching mechanisms on the speed of the populations, including constant, ECM-dependent, 220
and density-dependent switching rates. 221

2.3 Other applications 222

Go-or-grow models have also been used in ecological contexts for the description of immobile 223
and dispersing populations and two-species competition settings. Studies of the “drift para- 224
dox”, where aquatic insects in streams with downstream drift are able to remain upstream, 225
have included two-phase models where an insect is either mobile in the stream (moving with 226
diffusion and advection) or stationary on the benthos (and reproducing), and insects transi- 227
tion between each phase [57, 76, 79–81, 92, 127, 132]. The benthic-drift model has also been 228
extended to study the movement of zebra mussels in rivers [58, 63]. Some models of predator- 229
prey systems or spreading of epidemics take on the form of two-equation reaction–diffusion 230
systems with one population as the prey or the susceptible population and the other as the 231
predator or the infected population, respectively [12, 28–30, 55, 56, 59, 60, 69, 75, 78, 135, 232
136]. Here, the populations only transition in one direction (from energy conversion from prey 233
to predator or transfer from susceptible to infected population) and both may be mobile. 234

Other examples of go-or-grow mechanisms in biological modeling studies include movement 235
of forest boundaries [15, 68], amoebae [17], genetically engineered microbes [72], cells during 236
wound healing [70], genetic traits [123], mRNA cargo [16], and bacteria [95]. 237

Further afield, studies of autocatalytic chemical reactions often include reaction–diffusion 238
equation systems with one-directional transitions and equal or differing diffusion constants for 239
the reactant and autocatalyst [6, 39, 85, 86, 102, 131]. The reaction terms in the autocatalytic 240
models inspired the form of the Klausmeier–Gray–Scott model, which examines stripe and 241
pattern formation of vegetation depending on water movement ([14, 105, 122]). 242

3 The go-or-grow model

243

In this section, we first introduce the classical FKPP equation [9, 71, 87], for which there is a vast developed literature and because it forms the basis for analysis of go-or-grow models due to their similar structure. Various go-or-grow models are subsequently stated, and the connection between the FKPP equation and go-or-grow models is demonstrated in the last subsection via the fast transition rate scaling.

244
245
246
247
248

3.1 FKPP equation

249

Letting $m(t, x)$ denote the population size at time $t \geq 0$ and spatial position $x \in \Omega \subset \mathbb{R}^k$, $k \geq 1$, then the FKPP reaction–diffusion equation reads

250
251

$$m_t = d\Delta m + f(m), \quad (1)$$

where the subscript t denotes the partial time derivative and Δ denotes the spatial Laplacian on Ω . Typically, $f(m)$ is of *logistic type*, i.e., it satisfies the following properties

252
253

$$f(0) = 0, \quad f(K) = 0, \quad f'(0) > 0, \quad f'(K) < 0, \quad \text{and } f(m) > 0 \text{ for } 0 < m < K, \quad (2)$$

where $K > 0$ denotes the carrying capacity. In addition, we will often consider the *substantial condition*, which is

254
255

$$f'(0)m \geq f(m), \quad \text{for } 0 \leq m \leq K. \quad (3)$$

In the following, we will use the notation $f(m) = g(m)m$, where $g(m)$ denotes the per-capita growth rate of the population $m(t, x)$.

256
257

3.2 Go-or-grow model types

258

Go-or-grow models can be seen as a generalization of the FKPP equation. We first define the general continuous go-or-grow model that represents the focus of this review, and then several special variations that are used to address some of the mathematical challenges described in the subsequent sections.

259
260
261
262

General go-or-grow model. Let $u(t, x)$ denote the density of migrating cells and $v(t, x)$ the density of stationary and proliferating cells. The *general go-or-grow model* is the system of equations

263
264
265

$$\begin{cases} u_t = d\Delta u - \mu u - \alpha(u, v)u + \beta(u, v)v, \\ v_t = g(u + v)v + \alpha(u, v)u - \beta(u, v)v, \end{cases} \quad (4)$$

where $d > 0$ is a constant diffusion coefficient, $\mu \geq 0$ is a natural death rate for the moving compartment, $\alpha(u, v)$ denotes the transition rate function from the moving cell compartment to the stationary one, and $\beta(u, v)$ denotes the transition rate function from the stationary cell compartment to the moving one. The function $g(u + v)v$ accounts for the proliferation of the cell population, and, in the literature, it often takes a logistic form.

266
267
268
269
270

Total population go-or-grow model. Starting from the general model (4), a first variation of it is obtained by assuming that the transition rates α and β depend on the sum of the two populations, i.e., $\alpha = \alpha(n)$ and $\beta = \beta(n)$, with

$$n(t, x) = u(t, x) + v(t, x). \quad (5)$$

This version of the go-or-grow model has been used in many papers (e.g. [34, 97, 117, 118, 121]). We refer to it as the total population go-or-grow model, whose equations are given by

$$\begin{cases} u_t = d\Delta u - \mu u - \alpha(n)u + \beta(n)v, \\ v_t = g(n)v + \alpha(n)u - \beta(n)v. \end{cases} \quad (6)$$

Balanced go-or-grow model. If we consider that the transition probabilities from moving to stationary compartment and from stationary to moving compartment are balanced in the total population model (6), i.e., $\alpha(n) + \beta(n) = 1$, we obtain the balanced go-or-grow model. Used in several works (e.g. [8, 97, 117]), its equations read

$$\begin{cases} u_t = d\Delta u - \mu u + \gamma[\Gamma(n)v - (1 - \Gamma(n))u], \\ v_t = g(n)v - \gamma[\Gamma(n)v - (1 - \Gamma(n))u], \end{cases} \quad (7)$$

where $\gamma > 0$ denotes the rate at which a switch happens and $\Gamma(n)$ and $(1 - \Gamma(n))$ are the probabilities that the switch is from moving to stationary compartment or vice versa, respectively.

Constant rates go-or-grow model. A further simplification of the previous models can be considered by assuming that the transition rates are constant, such as in [37, 42, 74]. We refer to this model as the constant rates go-or-grow model, which reads

$$\begin{cases} u_t = d\Delta u - \mu u - \alpha u + \beta v, \\ v_t = g(u + v)v + \alpha u - \beta v. \end{cases} \quad (8)$$

The constant rates model (8) may be seen as a special case of the balanced model (7) by setting

$$\gamma = \alpha + \beta \quad \text{and} \quad \Gamma = \frac{\beta}{\alpha + \beta}. \quad (9)$$

Analogously, the balanced model (7) may be seen a special case of the total population model (6) using the same assumption (9) and considering the rate γ depending on the total population.

For later use, it is useful to write the above models in vector form as

$$\mathbf{w}_t = D\Delta \mathbf{w} + \mathbf{F}(\mathbf{w}), \quad (10)$$

where $\mathbf{w} = (u, v)^T$, $D = \text{diag}(d, 0)$, and

$$\mathbf{F}(\mathbf{w}) = \begin{pmatrix} -\mu u - \alpha(u, v)u + \beta(u, v)v \\ g(u + v)v + \alpha(u, v)u - \beta(u, v)v \end{pmatrix}. \quad (11)$$

In this formulation, (10) clearly resembles (1).

3.3 Fast transition rate scaling

294

We begin by reviewing a well-known scaling technique used to connect the mathematical properties of the go-or-grow type of models with the classical FKPP equation (1). The *fast transition rate scaling* is based on the natural assumption that the transitions between stationary and moving states are fast as compared to proliferation and diffusion. Letting $\varepsilon > 0$ be a small parameter, we consider the general go-or-grow model (4) with fast transition rates $\alpha \sim \alpha/\varepsilon$ and $\beta \sim \beta/\varepsilon$, resulting in

295
296
297
298
299
300

$$\begin{cases} u_t = d\Delta u - \mu u - \frac{1}{\varepsilon} (\alpha(u, v)u - \beta(u, v)v), \\ v_t = g(u + v)v + \frac{1}{\varepsilon} (\alpha(u, v)u - \beta(u, v)v). \end{cases} \quad (12)$$

We introduce the regular perturbation expansion of $u(t, x)$ and $v(t, x)$,

301

$$\begin{aligned} u(x, t; \varepsilon) &= u_0(t, x) + \sum_{n=1}^{\infty} u_n(t, x)\varepsilon^n, \\ v(x, t; \varepsilon) &= v_0(t, x) + \sum_{n=1}^{\infty} v_n(t, x)\varepsilon^n, \end{aligned}$$

and we assume that α , β , and g are of order $O(1)$ and sufficiently smooth to allow for a Taylor expansion about (u_0, v_0) . Further assuming that each order of ε -terms vanishes independently, the zeroth order of ε reads

302
303
304

$$-\alpha(u_0, v_0)u_0 + \beta(u_0, v_0)v_0 = 0, \quad (13)$$

while the first order of ε gives

305

$$\begin{aligned} (u_0)_t &= d\Delta u_0 - \mu u_0 - \alpha(u_0, v_0)u_1 + \beta(u_0, v_0)v_1 \\ &\quad - (u_1, v_1) \cdot \nabla_{uv}\alpha(u_0, v_0)u_0 + (u_1, v_1) \cdot \nabla_{uv}\beta(u_0, v_0)v_0, \end{aligned} \quad (14a)$$

$$\begin{aligned} (v_0)_t &= g(u_0 + v_0)v_0 + \alpha(u_0, v_0)u_1 - \beta(u_0, v_0)v_1 \\ &\quad + (u_1, v_1) \cdot \nabla_{uv}\alpha(u_0, v_0)u_0 - (u_1, v_1) \cdot \nabla_{uv}\beta(u_0, v_0)v_0, \end{aligned} \quad (14b)$$

where ∇_{uv} is used to distinguish the derivatives with respect to u and v from the spatial derivatives. Summing (14a) and (14b), and then together with (13), we get the system

306
307

$$\begin{cases} (u_0 + v_0)_t = (d\Delta - \mu)u_0 + g(u_0 + v_0)v_0, \\ -\alpha(u_0, v_0)u_0 + \beta(u_0, v_0)v_0 = 0. \end{cases} \quad (15)$$

The second equation in (15) is an implicit equation for u_0 and v_0 . We can use the implicit function theorem to find v_0 as a function of u_0 if

308
309

$$\frac{\partial\beta(u_0, v_0)}{\partial v_0}v_0 + \beta(u_0, v_0) - \frac{\partial\alpha(u_0, v_0)}{\partial v_0}u_0 \neq 0.$$

For particular forms of the transition rate functions α and β , it is possible to explicitly compute the inverse function.

310
311

The first example of using the fast-transition rate scaling in go-or-grow models appears in [46] for the constant rates model (8). Under this model, it is possible to simplify system (15) to a single equation for the total population n , obtaining a convex combination of diffusion and growth as

$$n_t = \frac{\beta}{\alpha + \beta} d\Delta n + \frac{\alpha}{\alpha + \beta} g(n) - \mu n. \quad (16)$$

Here, the ratios $\beta/(\alpha + \beta)$ and $\alpha/(\alpha + \beta)$ represent the average fractions of the total cell population that belongs to the moving and stationary phase, respectively.

In the context of the total population go-or-grow model (6), an example of fast-transition rate scaling is done in [34] with $\mu = 0$ and $d = 1$. The following single governing equation in terms of the total population n is obtained:

$$n_t = \nabla \cdot (D(n)\nabla n) + \frac{\alpha(n)}{\alpha(n) + \beta(n)} n(1 - n), \quad (17)$$

where the density-dependent diffusion takes the form

$$D(n) = \frac{\alpha(n)\beta'(n) - \alpha'(n)\beta(n)}{(\beta(n) + \alpha(n))^2} \frac{\beta(n)}{\beta(n) + \alpha(n)}. \quad (18)$$

The natural assumptions that $\alpha(n)$ is a non-increasing function of the total cell density and $\beta(n)$ is a non-decreasing function guarantee that $D(n) \geq 0$ for any $n \geq 0$. If α and β are constant, we return to equation (16), which is of FKPP type (1). Moreover, under the assumption that cells remain proliferative at low densities, i.e., $\beta(0) = 0$, a diffusion coefficient is obtained which resembles typical non-linear equations with degenerate diffusion.

Finally, in [104], the authors compare a go-or-grow type model to a single-population model, showing how the single-population model replicate key features of glioblastoma progression. While their go-or-grow model includes switching functions based on factors other than cell density, it is important to note that the parameters used for comparison in the go-or-grow model (see Table 2 in [104]) are an order of magnitude larger than the other rates. This discrepancy satisfies the assumption of the fast transition rate approximation, which helps explain why the simulation results from both models are similar.

4 A general existence result

All the models introduced in the previous section are based on the coupling of an ordinary differential equation with a reaction–diffusion equation. It is possible to prove a general existence result by using the existence theory for mixed type equations presented by Rothe in [101]. Here, we recall the main assumptions and definition.

Let us consider system (4) in the form

$$\begin{cases} u_t = d\Delta u - du + (d - \mu)u - \alpha(u, v)u + \beta(u, v)v, \\ v_t = g(u + v)v + \alpha(u, v)u - \beta(u, v)v, \end{cases} \quad (19)$$

where we explicitly write the terms $-du + du$ so that $d(\Delta - 1)$ can be identified as a generator that has no eigenvalue equal to 0 in typical Neumann and periodic boundary conditions. In the case of Dirichlet boundary conditions, we do not need to use this trick and instead consider $d\Delta$ as the generator.

Definition 1. A mild solution (u, v) of (19) satisfies

344

$$\begin{aligned} (u, v) &\in L^\infty([0, T] \times \Omega)^2 \\ u(\cdot, t) &= S(t)u_0 + \int_0^t S(t-s) \left((d-\mu)u(s) - \alpha(u(s), v(s))u(s) + \beta(u(s), v(s))v(s) \right) ds \\ v(\cdot, t) &= v_0 + \int_0^t g(u(s) + v(s))v(s) + \alpha(u(s), v(s))u(s) - \beta(u(s), v(s))v(s) ds \end{aligned}$$

where $u(s) = u(\cdot, s)$ and $v(s) = v(\cdot, s)$, while $S(t)$ denotes the semigroup generated by $d(\Delta - 1)$ on $L^\infty(\Omega)$ with the boundary conditions (20c) defined below.

345
346

Let us introduce the following set of assumptions.

347

- $\Omega \subset \mathbb{R}^n$ is a smooth bounded domain with Hölder continuous boundary, i.e.,

$$\partial\Omega \in C^{2+\alpha}, \quad \alpha \in (0, 1). \quad (20a)$$

- The initial conditions satisfy $\bar{u}_0, \bar{v}_0 \in L^\infty(\Omega)$.

$$(20b)$$

- There are differentiable functions $a(x) \geq 0$, $b(x) \geq 0$, $a(x)$ and $b(x)$ not simultaneously equal to 0, such that for all $x \in \partial\Omega$,

$$b(x)u(t, x) + a(x) \frac{\partial}{\partial n} u(t, x) = 0,$$

where n denotes the outer normal vector on $\partial\Omega$.

$$(20c)$$

- For each bounded set $B \in \mathbb{R}^2$, there exists a constant C_B such that for all $(u, v), (w, y) \in B$,

$$\begin{aligned} |g(u+v) + \alpha(u, v) + \beta(u, v)| &\leq C_B, \\ |g(u) - g(w)| &\leq C_B |u - w|, \\ |\alpha(u, v) - \alpha(w, y)| &\leq C_B (|u - w| + |v - y|), \\ |\beta(u, v) - \beta(w, y)| &\leq C_B (|u - w| + |v - y|). \end{aligned} \quad (20d)$$

- The functions $g, \alpha, \beta \in C^2$; moreover, $\bar{u}_0 \in C^{2+\alpha}$, $\bar{v}_0 \in C^\alpha$, and \bar{u}_0 satisfies the boundary conditions (20c).

$$(20e)$$

Theorem 1. [Theorem 1 in [101] (pages 111-112)] Assume (20a)–(20d), then (4) has a unique mild solution which is bounded in L^∞ . If the maximal time of existence $T_{max} < \infty$, then

348
349
350

$$\lim_{t \rightarrow T_{max}} \|(u(t, x), v(t, x))\|_\infty = \infty.$$

Moreover, if (20e) holds, then, for all $T < T_{max}$, the solutions are classical with

351

$$u \in C^{2+\alpha, 1+\alpha/2}(\bar{\Omega} \times [0, T]), \quad v \in C^{\alpha, 1+\alpha/2}(\bar{\Omega} \times [0, T]).$$

Theorem 1 applies to all our variants of the go-or-grow models (4)–(8) with appropriate adjustments in the assumptions on the parameters. If a small diffusion term ($\epsilon\Delta v$) is considered in the equation for the proliferative population, e.g., as done in [10], then standard semigroup methods can be applied to find solutions to the system (see [50, 100]).

352
353
354
355

5 Instabilities and pattern formation

356

It is time to meet the monster on a leash. Marciniak-Czochra and collaborators have worked intensively on systems of reaction–diffusion equations coupled to ODEs [47, 82]. In the study of Turing-like pattern formation, they made an interesting discovery, which is that all smooth patterns are unstable, and non-constant steady states need to have jumps. They also found that high frequencies are unstable in the linearization. This has far-reaching consequences, also for our study here, as we will outline in this section.

357
358
359
360
361
362

5.1 The general case

363

The ability of reaction–diffusion systems to form spatial patterns is a well researched area [9, 71, 88, 120]. In a typical activator-inhibitor situation, for example, we consider a system of two reaction–diffusion equations, where one species is the activator and the other the inhibitor. Turing patterns arise for a short range activator and a long range inhibitor [9, 71, 88, 120]. The extreme situation would be a fully local activator, i.e., an activator without a diffusion term in the equations, leading to an ODE coupled to the PDE of the inhibitor. Hence, it is natural to expect that ODE-PDE systems can generate diffusion driven instabilities [47, 82], and we review some of the results here.

364
365
366
367
368
369
370
371

For a coupled system of the form

372

$$\begin{cases} u_t = d_u \Delta u + k(u, v), \\ v_t = h(u, v), \end{cases} \quad (21)$$

on a smooth domain with standard boundary conditions, a necessary and sufficient condition for diffusion driven instability at a steady state (\bar{u}, \bar{v}) is the autocatalysis condition

373
374

$$\frac{\partial h}{\partial v}(\bar{u}, \bar{v}) > 0. \quad (22)$$

A proof is given in Theorem 4 in [82], and we sketch some of the important steps here. If we abbreviate the partial derivatives at steady state as

375
376

$$k_u = k_u(\bar{u}, \bar{v}), \quad k_v = k_v(\bar{u}, \bar{v}), \quad h_u = h_u(\bar{u}, \bar{v}), \quad h_v = h_v(\bar{u}, \bar{v}),$$

then the Jacobian of the kinetic part of (21) evaluated at (\bar{u}, \bar{v}) , together with its trace and determinant is

377
378

$$A := \begin{pmatrix} k_u & k_v \\ h_u & h_v \end{pmatrix}, \quad \text{tr} A = k_u + h_v, \quad \det A = k_u h_v - k_v h_u.$$

To study diffusion-driven instability, we assume that (\bar{u}, \bar{v}) is stable for the kinetic part, i.e.

379

$$\text{tr} A < 0 \quad \text{and} \quad \det A > 0. \quad (23)$$

We linearize the full system (21) at the homogeneous steady state (\bar{u}, \bar{v}) , and we use the Fourier transform with dual variable ω . The dual variable ω plays the role of the mode. For example, if we restrict on a given interval $[0, L]$, then we have only discrete modes $\omega_n = \frac{n\pi}{L}$ for $n \in \mathbb{N}$. The use of an abstract variable ω here allows us to make the following calculations as if ω were a continuous variable, while later, we can restrict to the discrete values ω_n . The Jacobian of (21) at (\bar{u}, \bar{v}) becomes

380
381
382
383
384
385

$$J = \begin{pmatrix} -d_u \omega^2 + k_u & k_v \\ h_u & h_v \end{pmatrix},$$

which has trace and determinant

386

$$\text{tr}J = -d_u\omega^2 + \text{tr}A < 0, \quad \det J = -d_u\omega^2 h_v + \det A.$$

Hence we observe diffusion driven instability if $\det J < 0$, i.e.,

387

$$\omega^2 > \frac{\det A}{d_u h_v}. \quad (24)$$

Under this assumption, we find the corresponding eigenvalues of J as

388

$$\lambda_{1,2} = \frac{\text{tr}A}{2} \pm \frac{1}{2}\sqrt{\text{tr}J^2 - 4\det J},$$

where $\lambda_1 > 0$ and $\lambda_2 < 0$. It is interesting to look at the unstable eigenvalue λ_1 as a function of the mode ω ,

389
390

$$\lambda_1(\omega) = \frac{1}{2}(-d_u\omega^2 h_v + \text{tr}A) + \frac{1}{2}\sqrt{(-d_u\omega^2 h_v + \text{tr}A)^2 - 4(-d_u\omega^2 h_v + \det A)}. \quad (25)$$

Using elementary calculations, we can show (skipping the details) that for

391

$$\omega = \bar{\omega} = \sqrt{\frac{\det A}{d_u h_v}},$$

we have $\lambda_1(\bar{\omega}) = 0$. Moreover, $\lambda_1(\omega)$ is strictly increasing for $\omega \geq \bar{\omega}$ and it goes into saturation

392

$$\lim_{\omega \rightarrow \infty} \lambda_1(\omega) = 2(2 - \text{tr}A) > 0.$$

Hence, $\lambda_1(\omega)$ has the qualitative form shown in Figure 2, which illustrates that higher modes are more unstable than smaller modes. This is the main reason why smooth non-constant steady states are unstable [47, 82]. Moreover, this observation also has direct consequences for numerical computation. Note that different choices of parameters than those chosen in Figure 2 give qualitatively the same form.

393
394
395
396
397

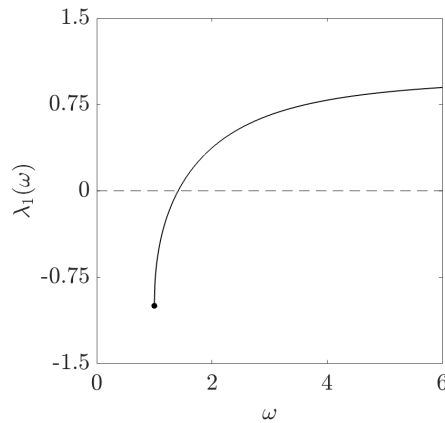


Figure 2: **Qualitative trend of $\lambda_1(\omega)$.** Typical form of the unstable eigenvalue $\lambda_1(\omega)$ computed from (25) as function of the mode ω . Here, the parameters are set to $d_u = 1$, $k_u = -2$, $k_v = -2$, $h_v = 1$, and $h_u = 2$.

Now, we consider a discretization of our domain with a step size Δx . Then the spatial frequency is Δx^{-1} . According to what we just observed for $\lambda_1(\omega)$, each mode $\omega > \Delta x^{-1}$

398
399

is unstable. For example, using homogeneous Neumann boundary conditions on an interval $[0, L]$, then $\omega_k = k\pi/L$ and each mode k with $\omega_k > \Delta x^{-1}$ is unstable. Hence, in the Neumann case, and also in other cases, small errors on the scale of the numerical discretization are amplified, making the numerics unstable. Reducing the step size does not help, as then higher modes are still unstable. This appears to be a principal challenge of the ODE-PDE coupled systems, and in such a situation, an accurate numerical solver is inconceivable. In Figure 3, we show a simulation of the balanced model (7) on a rectangular domain of size $[0, 50] \times [0, 50]$ for the transition and growth functions

$$\Gamma(n) = \frac{1}{2} (1 + \tanh[\nu(n^* - n)]), \quad g(n) = r \left(1 - \frac{n}{K}\right). \quad (26)$$

In this case, the above conditions (22), (23), and (24) for diffusion-driven instability are satisfied. We simulate the system (7) by using the method of lines and discretizing in space using a hybrid finite volume finite difference scheme, adapted from [119]. The solution converges to a smooth solution for u and a spatial pattern for v that is on the size of the discretization.

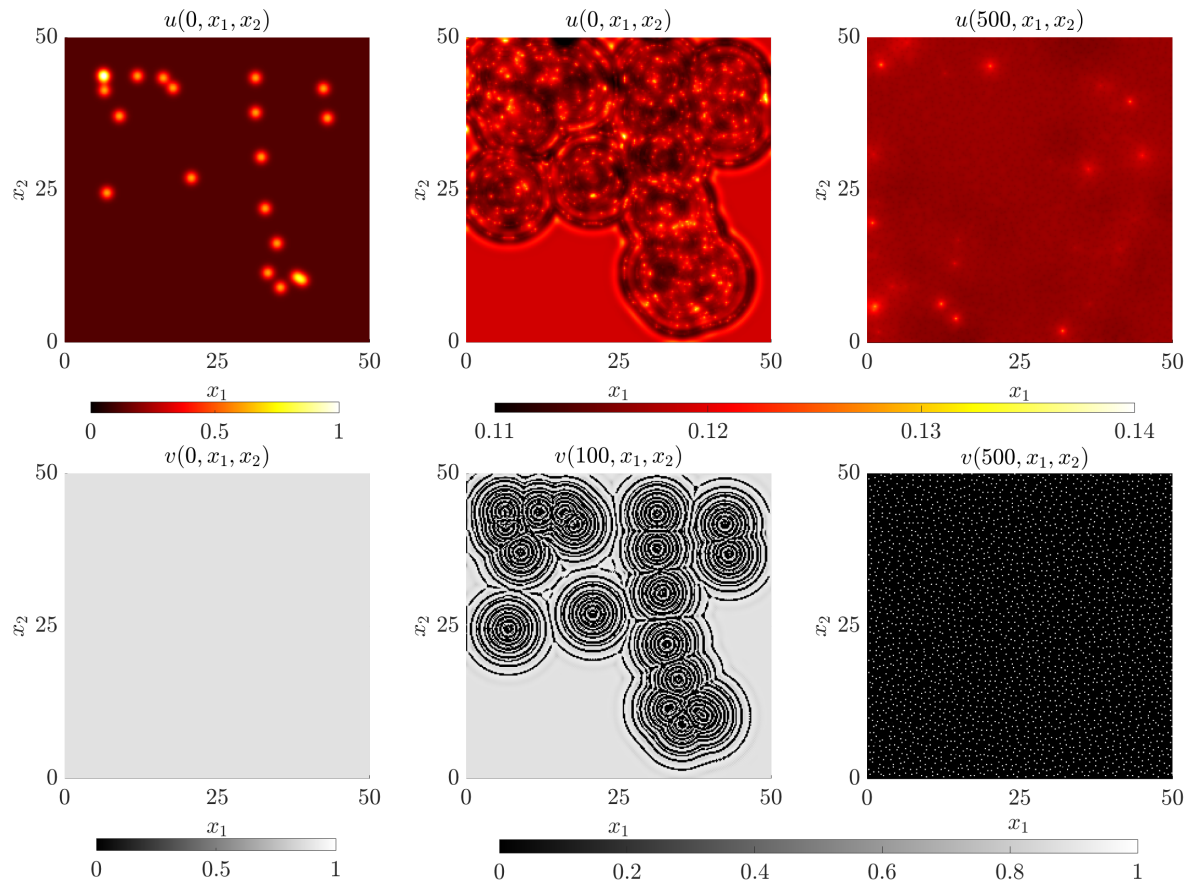


Figure 3: **Example of 2D instabilities emerging from model (7).** Two-dimensional simulations of the balanced model (7) on a rectangular domain of size $[0, 50] \times [0, 50]$ for the transition and growth functions (26). The first row shows the evolution of the population $u(t, x)$, while the second row illustrates $v(t, x)$, with $x = (x_1, x_2)$. The three columns illustrate the population behavior at $t = 0, 100, 500$, respectively. The regular mesh size is set to $\Delta x_1 = \Delta x_2 = 0.2$, while the parameter values are chosen as $\nu = 4$, $K = 1$, $r = 1$, $\gamma = 1.6$, $n^* = 0.75$, and $d = 1$.

To further analyze the impact of the discretization, we illustrate in Figure 4 the final state of the v variable when we reduce or enlarge Δx . We clearly see that the solution depends on

the choice of Δx . We admit that normally, when a solution depends on the discretization, it implies that the numerical method is not good enough. But as we describe earlier, this is not due to an inappropriate numerical solver, rather, it is a systematic problem of this kind of models.

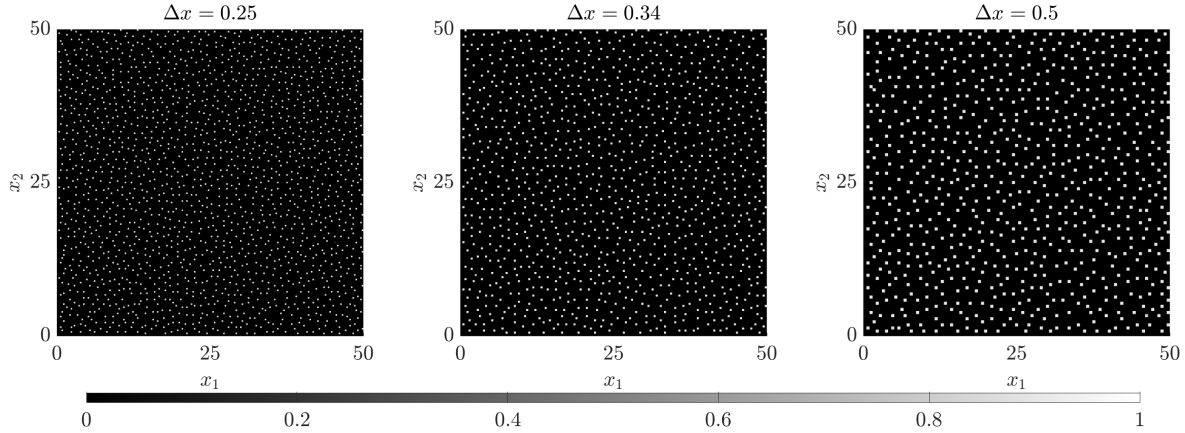


Figure 4: **Example of 2D instabilities emerging from model (7)**. Two-dimensional simulations at time $t = 500$ of the population $v(t, x)$, with $x = (x_1, x_2)$, for the balanced model (7) for three increasing value of the mesh size: $\Delta x = 0.25, 0.34, 0.5$. Here $\Delta x = \Delta x_i$, for $i = 1, 2$. The model is simulated on a rectangular domain of size $[0, 50] \times [0, 50]$ for the transition and growth functions (26). Parameters values are set to $\nu = 4$, $K = 1$, $r = 1$, $\gamma = 1.6$, $n^* = 0.75$, and $d = 1$.

5.2 The go-or-grow case

Let us now employ the above results for go-or-grow models. Turing patterns for go-or-grow were previously considered by Pham et al. [97] for the balanced model (7). The function $g(n)$ is assumed to be non-increasing ($g' \leq 0$ with $g(1) = 0$). In this case, we have two homogeneous steady states, $(0, 0)$ and $(\Gamma(1), 1 - \Gamma(1))$. We assume that $(0, 0)$ is linearly unstable, such that a tumor can indeed grow, and consider diffusion driven instabilities at $(\Gamma(1), 1 - \Gamma(1))$. Checking the autocatalysis condition (22), a necessary and sufficient condition for diffusion driven instability is

$$\gamma(\Gamma(1) + \Gamma'(1)) - g'(1)(1 - \Gamma(1)) < 0. \quad (27)$$

This condition was derived by Pham et al. [97] for the special choice of $g(n) = 1 - n$. Note that since g is assumed to be non-increasing, an increasing probability function $\Gamma(n)$ can never satisfy (27). However, a decreasing function $\Gamma(n)$ with $|\Gamma'(n)|$ large enough can satisfy (27).

Performing a linear stability analysis of the balanced model (7), we find that under condition (27) all unstable modes ω satisfy (24), which in this context becomes

$$\omega^2 > \frac{\gamma g'(1)(1 - \Gamma(1))}{\gamma(\Gamma(1) + \Gamma'(1)) - g'(1)(1 - \Gamma(1))}. \quad (28)$$

Note that we use again the mode ω as a continuous variable here. If we consider the balanced model (7) on an interval $[0, L]$ with homogeneous Neumann or Dirichlet boundary conditions, then the modes become $\omega_n = n\pi/L$.

For the probability of switching from stationary to moving [97], there are two choices:

- *Attractive case:* $\Gamma(n)$ is a decreasing smooth step function connecting $\Gamma(n) \approx 1$ for small n to $\Gamma(n) \approx 0$ for large n . Specifically,

$$\Gamma(n) = \frac{1}{2}(1 + \tanh(\nu(n^* - n))),$$

where n^* is the population size such that $\Gamma(n^*) = 0.5$. In this case, cells are more motile at low densities and more stationary at high densities.

- *Repulsive case:* $\Gamma(n)$ is an increasing smooth step function connecting $\Gamma(n) \approx 0$ for small n to $\Gamma(n) \approx 1$ for large n . Specifically,

$$\Gamma(n) = \frac{1}{2}(1 - \tanh(\nu(n^* - n))).$$

Cells are more motile at high densities and less motile at low densities.

In the repulsive case, we have $\Gamma' > 0$ and condition (27) cannot be satisfied, but in the attractive case, we have $\Gamma' < 0$ and for sufficiently large ν , condition (27) can be satisfied. Pham et al. [97] show numerical simulations for the attractive case that leads to spatial pattern formation and irregular traveling waves. However, Pham et al. [97] do not discuss the high level of instability in their numerics. In Figure 5, we show our own simulations of the traveling invasion waves of Pham et al. [97]. As in Figures 3–4, we observe instabilities behind the wave on the scale of the discretization. Hence, we can not ensure that the numerical solver is correct in those cases.

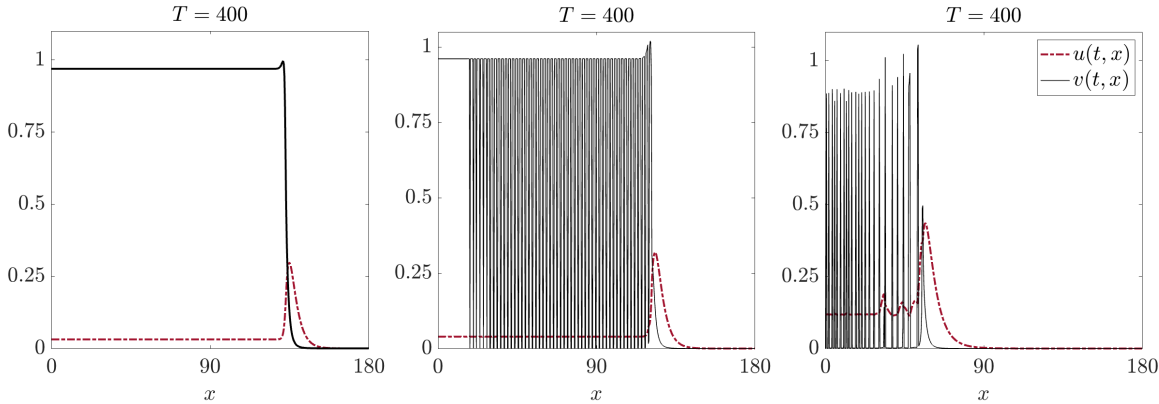


Figure 5: **Examples of 1D instabilities from model (7).** One-dimensional simulations of the balanced model (7) on the domain $[0, 180]$ for the transition and growth functions (26). The value of n^* is increased from left to right: $n^* = 0.57$, $n^* = 0.6$, and $n^* = 0.75$. The other parameters are set to $\nu = 4$, $K = 1$, $r = 1$, $\mu = 1.6$, and $d = 1$.

We have highlighted the rich array of intriguing mathematical properties related to the emergence of unusual behaviors and instabilities within the proposed framework. In the following, we focus on two well-established mathematical aspects for which more conclusive results can be obtained: the critical domain size problem and the traveling wave analysis.

6 Critical domain size

A common focus in spatial ecology is to identify the minimal size of a habitat such that a species has enough resources to survive, known as the critical domain size [9, 27, 71, 88]. This

has relevance in determining how large a habitat must be for species survival or how small it must be so that a parasite cannot establish itself.

6.1 The FKPP case

We first review the analysis of the critical domain size for the FKPP equation (1) under homogeneous Dirichlet boundary conditions. We look for nontrivial steady states, which are nonnegative solutions of the boundary value problem,

$$\begin{cases} -d\Delta m = g(m)m & \text{in } \Omega, \\ m = 0 & \text{on } \partial\Omega, \end{cases} \quad (29)$$

where $\Omega \subset \mathbb{R}^n$ is a bounded domain with a smooth boundary $\partial\Omega$. We denote by $\lambda_1(\Omega)$ the value of the leading eigenvalue of $-\Delta$ on Ω . This eigenvalue often plays an important role in growth phenomena on a given domain, and it will be the determining value here. In particular, there is a bifurcation in the behavior of solutions of (29) based on the size of the principal eigenvalue and the growth rate of the population at zero, i.e., $g(0)$.

Theorem 2 (Theorems 4.60–4.61 in [9]). *If the growth function $g \in C^2(\mathbb{R})$ is of logistic type (2), and satisfies the subtangential condition (3), then we have two cases:*

1. *If $\lambda_1(\Omega) \leq \frac{g(0)}{d}$, then (29) has a nontrivial solution;*
2. *If $\lambda_1(\Omega) > \frac{g(0)}{d}$, then (29) only has the trivial solution.*

This general result leads to the question of how the leading eigenvalue λ_1 depends on the domain size, which is clarified in the following theorem.

Theorem 3 (Theorem 2.21 in [125]). *For the eigenvalue problem associated with $-\Delta$, $\lambda_1(\Omega)$ is strictly decreasing with respect to Ω , in the sense that if $\Omega \subset \tilde{\Omega}$, then $\lambda_1(\Omega) \geq \lambda_1(\tilde{\Omega})$, and $\Omega \subsetneq \tilde{\Omega}$ implies $\lambda_1(\Omega) > \lambda_1(\tilde{\Omega})$.*

The dependency on the domain size may furthermore be made more explicit by looking at the one-dimensional setting. Setting $\Omega = [0, L]$, then the eigenvalue is $\lambda_1 = (\pi/L)^2$, and we can rewrite Theorem 2 in the following manner.

Corollary 4. *If $\Omega = [0, L]$, $g \in C^2(\mathbb{R})$, and g is of logistic type (2) and satisfies the subtangential condition (3), then we have two cases:*

1. *If $L \geq \pi\sqrt{\frac{d}{g(0)}}$, then (29) has a nontrivial solution;*
2. *If $L < \pi\sqrt{\frac{d}{g(0)}}$, then (29) only has the trivial solution.*

In this one-dimensional setting, we have a clear bifurcation in the behavior of solutions based on the domain size L , and denote the bifurcation value for L the critical domain size:

$$L_{crit} = \pi\sqrt{\frac{d}{g(0)}}. \quad (30)$$

6.2 The go-or-grow case

486

Returning to the go-or-grow model (4), similarly to the previous section, we look for nontrivial steady states, which will be nonnegative solutions of the following boundary value problem

487

488

$$\begin{cases} -d\Delta u = -\mu u - \alpha(u, v)u + \beta(u, v)v, & \text{in } \Omega, \\ g(u + v)v + \alpha(u, v)u - \beta(u, v)v = 0, & \text{in } \Omega, \\ (u, v) = (0, 0), & \text{on } \partial\Omega, \end{cases} \quad (31)$$

where Ω is a bounded domain with a smooth boundary.

489

The critical domain size problem for the case where α and β are constant (the constant rates go-or-grow model (8)) was studied in [46], where the following result was proven.

490

491

Theorem 5 (Theorem 4 in [46]). *Consider (31) with constant rates α and β . If $g \in C^2(\mathbb{R})$, and g is of logistic type (2) and satisfies the subtangential condition (3), then we have three cases:*

492

493

494

1. Assume $\beta > g(0)$ and

495

$$\lambda_1(\Omega) < \frac{1}{d} \left(\frac{\alpha g(0)}{\beta - g(0)} - \mu \right), \quad (32)$$

then there exists a nontrivial steady state solution;

496

2. Assume $\beta > g(0)$ and

497

$$\lambda_1(\Omega) > \frac{1}{d} \left(\frac{\alpha g(0)}{\beta - g(0)} - \mu \right), \quad (33)$$

then the steady state is zero;

498

3. If $\beta < g(0)$, then the zero solution is always unstable, and nontrivial steady states exist.

499

Similar to the FKPP case, we have a bifurcation that is based on the domain size in cases 1 and 2. The threshold in (32)–(33) depends on the growth rate and, somewhat unsurprisingly, on the transition rates α and β and the death rate μ . What is surprising is that a third case appears for a small transition rate β . If the growth rate of the v population at 0 is greater than the transition rate out of the v compartment, i.e., $\beta < g(0)$, then there is no critical domain or bifurcation on the domain size. This means that for any size or shape of domain Ω , there exist nontrivial populations of u and v .

500

501

502

503

504

505

506

This property is another example of the unexpected properties of the go-or-grow systems. In fact, we can link this case to the autocatalysis condition (22) discussed earlier. If we compute (22) for the constant rates model (8), we find indeed

507

508

509

$$\left. \frac{\partial h}{\partial v} \right|_{(u,v)=(0,0)} = g(0) - \beta > 0.$$

In the autocatalysis case where $\beta - g(0) > 0$, we can directly relate the results from Theorem 2 and Theorem 5 for $\Omega = [0, L]$ and $\mu = 0$. The threshold condition (33) can be written as a condition for the domain length L

510

511

512

$$L > L_{\text{crit}} = \pi \sqrt{\frac{d(\beta - g(0))}{g(0)\alpha}} = \pi \sqrt{\frac{d}{g(0)}} \underbrace{\sqrt{\frac{\beta - g(0)}{\alpha}}}_{K_{\alpha\beta}}. \quad (34)$$

In this example, the critical domain of FKPP (30) and the critical domain of the constant rates go-or-grow model (34) are related by the factor $K_{\alpha\beta}$. Setting $K_{\alpha\beta} = 1$ gives the equation when the two critical domains are equal, $\alpha + g(0) = \beta$. If we increase the transition rate to the moving population, β , or decrease the transition rate to the growing population, α , from the $K_{\alpha\beta} = 1$ values, the critical domain of the go-or-grow model will be larger than the critical domain of FKPP. Similarly, if we reduce β or increase α , the critical domain of the go-or-grow model will be smaller than the critical domain of FKPP.

7 Traveling wave analysis and invasion speeds

To quantify the spread of populations in terms of the speed of invasion, traveling wave analysis has become a widely adopted approach, with a particular focus on determining the existence of traveling waves and their minimum speed. This is due to the fact that both the FKPP equation (1) and go-or-grow models (4) inherently describe situations where waves of population density propagate at a constant speed.

7.1 The FKPP case

The analysis of traveling waves for the FKPP equation (1) is a well-researched and well-described textbook method [9, 71, 73, 87, 108]. Consider (1) on the real line and assume the growth function f is of logistic type (2), we introduce the *traveling wave coordinate* $z = x - ct$ with *wave speed* c , and define a traveling wave solution to be a self-similar solution of the form $m(t, x) = M(z)$. Substituting this ansatz into (1) yields a second-order ODE for M of the form

$$-cM' = dM'' + g(M)M, \quad (35)$$

with boundary conditions $M(-\infty) = 1$ and $M(\infty) = 0$. This ODE can be analyzed with phase plane methods, where a traveling wave of (1) corresponds to a heteroclinic connection between two equilibria in the phase space. This heteroclinic connection depends on the choice of the speed c . As done in [9, 71, 73, 87, 108], it can be shown that, under the subtangential condition (3), the minimum wave speed is

$$\bar{c}_{\text{FKPP}} = 2\sqrt{dg(0)}.$$

7.2 The go-or-grow case

As in the FKPP case, traveling wave solutions for go-or-grow models can be seen as connections between two equilibria of the system. Ahead of the wave, we find the trivial equilibrium $(u, v) = (0, 0)$, while at the back of the wave we typically see a coexistence equilibrium (u^*, v^*) . To ensure these states exist, we make the following assumption:

- g is a continuous function that is differentiable at 0 and 1, it has one root at $n = 1$, and $g(n)n \leq g(0)n$ for $0 \leq n \leq 1$; (36a)

- there is only one non-zero solution $(u^*, v^*) \in \mathbb{R}_+^2$ of the system (36b)

$$\begin{cases} 0 = -\mu u^* - \alpha(u^*, v^*)u^* + \beta(u^*, v^*)v^*, \\ \mu u^* = g(u^* + v^*)v^*. \end{cases}$$

Assumptions (36a)-(36b) guarantees that $\mathbf{F}(0,0) = \mathbf{F}(u^*,v^*) = (0,0)$ in (10), allowing us to formalize the question of a traveling wave with the following definitions. 543
544

Definition 2. Consider the general go-or-grow model (4) and introduce the traveling wave coordinate $z = x - ct$ for a fixed speed c . A solution of the form $u(t,x) = U(x - ct)$ and $v(t,x) = V(x - ct)$ is called a traveling wave solution with speed c . The traveling wave is called a wavefront if $(U(z), V(z))$ has limits 545
546
547
548

$$\lim_{z \rightarrow +\infty} (U(z), V(z)) = (0, 0), \quad \lim_{z \rightarrow -\infty} (U(z), V(z)) = (u^*, v^*).$$

If $c > 0$, the invading traveling wave moves to the right, while if $c < 0$, the invading traveling wave moves to the left. 549
550

There are two distinct notions for the wave speed, c , which are relevant in our analysis. 551

Definition 3. 552

- The nonlinear spread rate, c^* , denotes the observed minimal spreading speed of solutions of the full nonlinear system (4). 553
554
- The linear spread rate, \bar{c} , denotes the spreading wave speed of the solutions of its linearization at the leading edge (see [46]). 555
556

Specifically, we say that the system is linearly determined if $c^* = \bar{c}$. 557

The first results for the existence of wave fronts and the expression for the corresponding spreading speed were obtained for the constant rates go-or-grow model (8) by Haderler, Lewis, and collaborators [46, 74]. The connection between nonlinear spread speed, c^* , and linear spread speed, \bar{c} , was established in the case that the function $g(u + v)$ only depends on the stationary population $g(v)$. 558
559
560
561
562

For the balanced go-or-grow model (7) with $g(n) = 1 - n$, Pham et al. [97] showed numerically that invasion waves exist with different qualitative behavior. In particular, the wake of the wave might be a homogeneous steady state, a periodic wave train, or even an irregular pattern, as we have shown in Section 5. 563
564
565
566

More recently, Falcó et al. [34] examined the minimum invasion speed in the case of the total population go-or-grow model (6) with no death rate ($\mu = 0$), logistic growth for the proliferating population ($g(n) = 1 - n$), and $\alpha(n)$ and $\beta(n)$ as nonincreasing and nondecreasing functions, respectively. By assuming $\alpha(n) > 0$ for all $n > 0$, they ensure the existence of only two equilibria in the system, 567
568
569
570
571

$$E_0 = (0, 0), \quad E_1 = \left(\frac{\beta(1)}{\alpha(1) + \beta(1)}, \frac{\alpha(1)}{\alpha(1) + \beta(1)} \right),$$

and find the traveling wave solutions as heteroclinic connections between these two equilibria in phase space. Moreover, considering the linearized version of (6) about the equilibrium E_0 and transforming to wave coordinates, they obtain the expression for the linear spread rate 572
573
574

$$\bar{c} = \inf_{\rho > 0} \frac{\rho^2 + 1 - \alpha(0) - \beta(0) + \sqrt{(\rho^2 + 1 - \alpha(0) - \beta(0))^2 - 4(1 - \beta(0))\rho^2 + 4\alpha(0)}}{2\rho}. \quad (37)$$

Although this formula still includes the infimum operation, it is observed that 575

$$\left. \frac{dc}{d\rho}(\rho) \right|_{\rho=1} = \frac{\beta(0) - \alpha(0)}{\alpha(0) + \beta(0)},$$

and thus, some special cases emerge. 576

• For $\alpha(0) = \beta(0)$, (37) obtains its minimum at $\rho = 1$, which implies that $\bar{c} = 1$. 577

• For $\beta(0) = 0$, it is possible to explicitly solve (37), obtaining 578

$$\bar{c} = \frac{1}{\sqrt{1 + \alpha(0)}}.$$

In this case, if $\beta(n) \neq 0$ for $n > 0$, it has been demonstrated that ensuring the positivity 579
of traveling wave solutions requires a wave speed $c > \bar{c}$. Therefore, for the case where 580
 $\beta(0) = 0$, the traveling wave solutions exhibit a wave speed greater than \bar{c} meaning that 581
the wave speed is nonlinearly determined. 582

• Similarly, if $\alpha(0) = 0$, 583

$$\bar{c} = \begin{cases} \sqrt{1 - \beta(0)}, & \text{if } \beta(0) < 1, \\ 0, & \text{otherwise.} \end{cases}$$

• When $\alpha(0) \neq \beta(0)$, $\bar{c} \leq c(1) = 1$. 584

Similar results for the total population go-or-grow model (6) were obtained in Stepien et 585
al. [111] in the case $\mu \neq 0$, assuming logistic growth with constant rate, r , and the following 586
specific forms for the transition functions, 587

$$\alpha(n) = \kappa \frac{K_v^k}{n^k + K_v^k}, \quad \beta(n) = \epsilon \kappa \frac{n^k}{n^k + K_u^k}, \quad (38)$$

with ϵ , κ , k , K_u , and K_v positive constants. A closed form for the dispersion relation was 588
obtained, which provides the minimum wave speed 589

$$\bar{c} = r \sqrt{\frac{d}{r + \kappa + \mu}}. \quad (39)$$

Moreover, the existence of a heteroclinic orbit in phase space that corresponds to the approx- 590
imate traveling wave (under certain conditions) was proven. 591

7.3 A unifying framework and a general result 592

The previous results can be cast into the framework of cooperative reaction–diffusion systems. 593
The lemmas and theorems presented here are new, and they are based on a general theory 594
of cooperative reaction–diffusion systems developed in [35, 77, 128]. The proofs require a 595
straightforward check of the general assumptions, which is presented in Appendix A. 596

Before we show the existence of traveling waves, we first characterize the wave speed \bar{c} 597
through the linearization at the leading edge. For this, we make the following assumptions: 598

- $\alpha(u, v)$ and $\beta(u, v)$ are piecewise continuously differentiable in (u, v) for $0 \leq u \leq u^*$ 599
and $0 \leq v \leq v^*$, differentiable at $(0, 0)$, and 600

$$(g(0) - \beta(0, 0))(\mu + \alpha(0, 0)) + \alpha(0, 0)\beta(0, 0) > 0;$$

(40a)

- For any $(u, v) \in [0, u^*] \times [0, v^*]$,

$$\alpha(u, v) + \frac{\partial}{\partial u}(\alpha(u, v))u + \frac{\partial}{\partial u}(g(u + v) - \beta(u, v))v \geq 0, \quad (40b)$$

and

$$\beta(u, v) + \frac{\partial}{\partial v}(\beta(u, v))v - \frac{\partial}{\partial v}(\alpha(u, v))u \geq 0.$$

Assumption (40a) gives regularity such that we can take the Jacobian at $(0, 0)$ and ensures that the Jacobian at $(0, 0)$ has a positive eigenvalue. Note that, if $\mu = 0$, the condition $(g(0) - \beta(0, 0))(\mu + \alpha(0, 0)) + \alpha(0, 0)\beta(0, 0) > 0$ is satisfied. The assumption (40b) is sufficient to ensure that (4) is cooperative.

We transform system (10) into wave coordinate $z = x - ct$ and linearize about $(0, 0)$ to obtain

$$-c\mathbf{w}' = D\mathbf{w}'' + \mathbf{F}'(0, 0)\mathbf{w}, \quad (41)$$

where $\mathbf{w} = (u, v)^T$, $D = \text{diag}(d, 0)$, \mathbf{F} is as defined in (11), and $\mathbf{F}'(0, 0)$ is the Jacobian of \mathbf{F} at $(0, 0)$. We write the solution of (41) as $\mathbf{w} = \nu e^{-\rho z}$, where ρ denotes the exponential decay rate at the leading edge and ν is an arbitrary vector. Substituting this ansatz into (41) yields the algebraic system

$$-c\rho\nu = D\rho^2\nu + \mathbf{F}'(0, 0)\nu.$$

Defining the matrix $A(\rho) = D\rho^2 + \mathbf{F}'(0, 0)$, we arrive at the eigenvalue problem given by

$$(A(\rho) - c\rho\mathbb{I})\nu = 0,$$

for the eigenvalue $\lambda_A = c\rho$. We find that the principal and positive eigenvalue of A is

$$\lambda_A(\rho) = \frac{d\rho^2 + g(0) - \mu - \alpha(0, 0) - \beta(0, 0)}{2} + \frac{\sqrt{[d\rho^2 + g(0) - \mu - \alpha(0, 0) - \beta(0, 0)]^2 + 4[(g(0) - \beta(0, 0))(\mu + \alpha(0, 0) - d\rho^2) + \alpha(0, 0)\beta(0, 0)]}}{2}, \quad (42)$$

with associated eigenvector

$$\nu(\rho) = \left(\frac{\lambda_A(\rho) - g(0) + \beta(0, 0)}{\alpha(0, 0)}, 1 \right)^T, \quad (43)$$

which is a positive vector for all $\rho \geq 0$. To find the minimum wave speed of the linearized system, \bar{c} , we take the minimum ratio of the eigenvalue and decay rate as

$$\bar{c} := \inf_{\rho > 0} \frac{\lambda_A(\rho)}{\rho}. \quad (44)$$

We verified that, under the assumptions $\mu = 0$, $\alpha = \alpha(n)$, and $\beta = \beta(n)$, condition (44) coincides with (37) derived in [34] for the total population model (6). Furthermore, when $\mu \neq 0$ and the transition functions are given by (38), condition (44) matches (39), which was previously derived in [111].

Lemma 6. Let α , β , and g satisfy (36b), (40a), and (40b) and consider the initial condition $\phi = (\phi_1, \phi_2) \in \mathcal{C}_{u^*, v^*} = \{(\phi_1, \phi_2) \in C(\mathbb{R}; \mathbb{R}^2) : 0 \leq \phi_1(z) \leq u^*, 0 \leq \phi_2(z) \leq v^* \forall z \in \mathbb{R}\}$. Let $\mathbf{w}(t, x; \phi) := (u(t, x; \phi_1), v(t, x; \phi_2))$ be the unique solution of (4) through ϕ . Then, there exists a real number c^* with $0 < c^* \leq \bar{c}$, such that the following statements are valid:

1. If ϕ has compact support, then $\lim_{\substack{t \rightarrow \infty \\ |x| \geq ct}} \mathbf{w}(t, x; \phi) = 0$, for all $c > c^*$;

2. For any $c \in (0, c^*)$ and $\mathbf{r} > \mathbf{0}$, there is a positive number $R_{\mathbf{r}}$ such that for any $\phi \in \mathcal{C}_{u^*, v^*}$ with $\phi \leq \mathbf{r}$ on an interval of length $2R_{\mathbf{r}}$, there holds $\lim_{\substack{t \rightarrow \infty \\ |x| \leq ct}} \mathbf{w}(t, x; \phi) = (u^*, v^*)$;

3. If, in addition, we have a linear bound for any $\eta > 0$, i.e.,

$$g(\eta(1 + \nu_1(\rho))) \leq -\alpha(\eta\nu_1(\rho), \eta)\nu_1(\rho) + \beta(\eta\nu_1(\rho), \eta) + \lambda_A(\rho) \leq g(0), \quad (45)$$

for all $\rho \in (0, \rho^*]$, then $c^* = \bar{c}$, where ρ^* is the value of ρ at which $\lambda_A(\rho)/\rho$ attains its infimum, and $\nu_1(\rho)$ is the first component of the eigenvector (43).

Proof. The proof is based on the general theory of [35, 77, 128] and is presented in Appendix A. \square

Lemma 6 provides sufficient conditions for the existence of a constant spreading speed of a compact initial condition in items 1 and 2. Item 3 gives conditions such that the model is linearly determined and that the nonlinear spread rate, c^* , coincides with the linearized spread rate, \bar{c} . However, to prove the existence of traveling waves, we also require condition (45) as well as the following assumption:

- There exist $a > 0$, $\sigma > 1$, and $\mathbf{r} > \mathbf{0}$ such that

$$\begin{aligned} (\alpha(0, 0) - \alpha(u, v))u + (\beta(u, v) - \beta(0, 0))v &\geq -a|u + v|^\sigma, \\ (g(u + v) - g(0))v - (\alpha(0, 0) - \alpha(u, v))u - (\beta(u, v) - \beta(0, 0))v &\geq -a|u + v|^\sigma, \end{aligned}$$

for all $\mathbf{0} \leq (u, v) \leq \mathbf{r}$.

(46)

Although condition (46) looks quite complex, it is already satisfied when $\mathbf{F}(u, v)$ is twice differentiable in both components [35]. The assumption (45) comes from a variant of the subtangential condition (3), requiring that $\mathbf{F}(u, v) \leq \mathbf{F}'(0, 0)$ along the direction of the eigenvector associated with the principal eigenvalue $\lambda_A(\rho)$. With assumptions (36b), (40a)–(40b), and (46)–(45), we can show that (4) has traveling wave solutions.

Theorem 7. If the general grow-or-grow model (4) satisfies the conditions (36b), (40a)–(40b), and (45)–(46), then for each $c < \bar{c}$, it has a nonincreasing wavefront $(U(x - ct), V(x - ct))$ connecting (u^*, v^*) to $(0, 0)$. However, for any $c \in (0, \bar{c})$, there is no wavefront $(U(x - ct), V(x - ct))$ connecting (u^*, v^*) to $(0, 0)$.

Proof. The proof requires a check that the conditions for the general theory of cooperative systems are satisfied, and it is presented in Appendix A. \square

Theorem 7 allows us to establish the existence of traveling wave solutions with a formula for the wave speed (44) for a large class of go-or-grow models. Although many go-or-grow models fall into the above framework, there exists plenty of examples that fail one of the

assumptions, such as those studied in [34, 111, 121] that numerically display traveling wave solutions, but they fail the cooperativity condition (40b). To prove traveling wave solutions in those cases, one can attempt to construct upper and lower solutions and use a fixed point proof, as done in [133–135], or use a geometric shooting method, as in [55, 56, 59, 60, 75, 78]. Another common method is to use approximations, such as the fast transition rate scaling introduced in Section 3.3, where the general go-or-grow model (4) can be transformed into a FKPP equation (1) for the total population depending on the form of the transition functions α and β . Since the FKPP equation (1) has traveling wave solutions and a simple formula for the spreading speed, the fast-transition scaling can provide an approximation on the spreading speed of (4).

7.4 Connection between the spread rate of the FKPP equation and go-or-grow models

To link the foundational analysis of the FKPP equation (1) as summarized in Section 7.1 with analysis of go-or-grow types of models (10) (Sections 7.2–7.3), we compare the spread rate between the cases.

Theorem 8. *Assume $\mu = 0$, $\mathbf{F}(\mathbf{w})$ is given by (11), and α , β , and g satisfy assumptions (2), (3), (36b), (40a)–(40b), and (45)–(46). Then the minimum wave speed, \bar{c} of the go-or-grow model (4) given by (44) satisfies the inequality*

$$\bar{c} \leq \frac{1}{2} \bar{c}_{\text{FKPP}} = \sqrt{dg(0)}. \quad (47)$$

Proof. Since $\mathbf{F}(u, v)$ satisfies assumptions (36b), (40a)–(40b), and (45)–(46), Theorem 7 can be applied, and we have that the minimum wave speed of the corresponding go-or-grow model is given by

$$\bar{c} = \inf_{\rho \geq 0} \frac{\lambda_+(\rho)}{\rho}, \quad (48)$$

where $\lambda_+(\rho)$ is the principal eigenvalue of the matrix

$$A = \begin{pmatrix} d\rho^2 & 0 \\ 0 & 0 \end{pmatrix} + \begin{pmatrix} -\alpha(0,0) & +\beta(0,0) \\ \alpha(0,0) & -\beta(0,0) + g(0) \end{pmatrix}. \quad (49)$$

This can be written explicitly as

$$\lambda_+(\rho) = \frac{d\rho^2 + g(0) - \alpha(0,0) - \beta(0,0)}{2} + \frac{\sqrt{(d\rho^2 + g(0) - \alpha(0,0) - \beta(0,0))^2 - 4(d\rho^2(g(0) - \beta(0,0)) - \alpha(0,0)g(0))}}{2}. \quad (50)$$

We notice that substituting the choice of $\rho = \sqrt{g(0)/d}$ into (50), we get

$$\frac{\lambda_+\left(\sqrt{\frac{g(0)}{d}}\right)}{\sqrt{\frac{g(0)}{d}}} = \sqrt{dg(0)}.$$

Thus, we have the set of inequalities

$$\bar{c} = \inf_{\rho \geq 0} \frac{\lambda_+(\rho)}{\rho} \leq \sqrt{dg(0)} \leq 2\sqrt{dg(0)} = \bar{c}_{\text{FKPP}}. \quad (51)$$

□ 673

Some special cases of this result were already proven in the literature for the constant rates model (8) in [37, 74] and for the total population model (6) in [34]. However, the results provided here are a generalization for the case of the general go-or-grow model (4). As an example, in Figure 6 we illustrate the traveling wave profile for the constant rates model (8) (black and red lines) and the FKPP model (1) (blue lines). These numerical simulations show how the FKPP model is at least two times faster than the constant rates go-or-grow model.

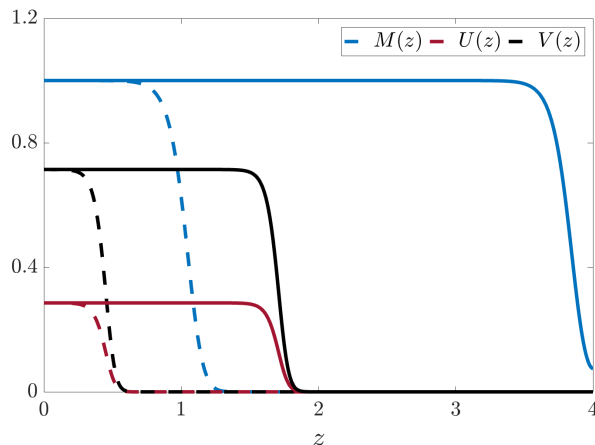


Figure 6: **Traveling wave profiles for models (1) and (8).** Traveling wave profiles for the FKPP model (1) ($M(z)$ in blue) and the constant rate go-or-grow (8) (moving cells $U(z)$ in red, proliferating cells $V(z)$ in black). Simulations are shown at two different time steps: an earlier time T_1 (dashed curves) and a later time T_2 (solid curves). Parameters are set to $\alpha = 1$, $\beta = 2$, $g(0) = 1$, $\mu = 0$, and $d = 0.0001$.

7.5 Large wave speed scaling

In addition to studying the wave speed of traveling wave solutions of the general go-or-grow model (4), here we introduce the large wave speed scaling approach, which provides insights into the shape of the traveling waves. Originally developed by Canosa [11], this method allows for an approximation of the traveling wave solution by considering an asymptotic expansion of the traveling wave system in the limit of large wave speeds. For systems for which no general traveling wave solution theory exists, i.e., those systems which are noncooperative and not bounded above and below by cooperative systems, this technique is a useful way to obtain the form of the traveling wave by solving a much simpler approximate system. Furthermore, this approach facilitates the investigation of the conditions under which the approximation aligns closely with the traveling wave system, providing a clearer understanding of the wave dynamics.

Introducing the traveling wave coordinate, $z = x - ct$, such that $U(z) = u(t, x)$ and $V(z) = v(t, x)$, the general go-or-grow model (4) is written as

$$\begin{cases} -cU' = DU'' - \mu U - \alpha(U, V)U + \beta(U, V)V, \\ -cV' = g(U + V)V + \alpha(U, V)U - \beta(U, V)V. \end{cases} \quad (52)$$

By using the scaling $\xi = -\frac{1}{c}z$, we obtain the approximation

694

$$\begin{cases} U' = \frac{D}{c^2}U'' - \mu U - \alpha(U, V)U + \beta(U, V)V, \\ V' = g(U + V)V + \alpha(U, V)U - \beta(U, V)V. \end{cases}$$

Defining the perturbation parameter $\delta := 1/c^2$ and assuming it is small, we expand U and V as regular perturbation expansions

695

696

$$U = \sum_{n=0}^{\infty} U_n \delta^n, \quad V = \sum_{n=0}^{\infty} V_n \delta^n.$$

As in the fast transition rate scaling (Section 3.3), we require that α , β , and g are sufficiently smooth to allow for a Taylor expansion at (U_0, V_0) . In addition, we require each order of δ to vanish independently. With both of these assumptions, the zeroth order of δ reads

697

698

699

$$\begin{cases} U'_0 = -\mu U_0 - \alpha(U_0, V_0)U_0 + \beta(U_0, V_0)V_0, \\ V'_0 = g(U_0 + V_0)V_0 + \alpha(U_0, V_0)U_0 - \beta(U_0, V_0)V_0. \end{cases} \quad (53)$$

The effective result of scaling is removing the diffusion term from the analysis, reducing the dimension of the phase space of the problem by one. In this case, we reduce the phase space to two dimensions, allowing for the examination of the shape of the traveling wave solutions.

700

701

702

Example We illustrate the large wave speed approximation in the case of the constant rates go-or-grow model (8) with $\mu = 0$ and logistic growth function, $g(u + v)v = (1 - (u + v))v$. In this example, system (53) becomes

703

704

705

$$\begin{cases} U'_0 = -\alpha U_0 + \beta V_0, \\ V'_0 = (1 - U_0 - V_0)V_0 + \alpha U_0 - \beta V_0. \end{cases} \quad (54)$$

The classical phase plane analysis shows that the origin $(0,0)$ is a saddle node and the equilibrium $(U_0^*, V_0^*) = \left(\frac{1}{\alpha/\beta+1}, \frac{\alpha/\beta}{\alpha/\beta+1}\right)$ is a stable node. We calculate the nullclines of the above system in terms of U_0 , obtaining

706

707

708

$$U_0\text{-nullcline:} \quad V_{\mathcal{N}_1}(U_0) = \frac{\alpha}{\beta}U_0, \quad (55a)$$

$$V_0\text{-nullcline:} \quad V_{\mathcal{N}_2}(U_0) = \frac{(1 - U_0) - \beta}{2} + \frac{\sqrt{((1 - U_0) - \beta)^2 + 4\alpha U_0}}{2}. \quad (55b)$$

From these nullclines, it is possible to define the trapping region

709

$$\mathcal{W} = \{(U_0, V_0) \in \mathbb{R}_+^2 : 0 \leq U_0 \leq U_0^*, V_{\mathcal{N}_1}(U_0) \leq V_0 \leq V_{\mathcal{N}_2}(U_0)\}. \quad (56)$$

Indeed, for trajectories on the line $\{U_0 = 0, V_0 > 0\}$, we have $U'_0 > 0$, thus they point inward into \mathcal{W} . Then, we consider the curve $\{V_0 = V_{\mathcal{N}_1}(U_0), 0 < U_0 < U_0^*\}$, whose trajectories have $U'_0 = 0$ and

710

711

712

$$V'_0 = \frac{\alpha}{\beta} \left[1 - \left(1 + \frac{\alpha}{\beta} \right) U_0 \right] U_0 > 0,$$

thus, the flux points upwards into \mathcal{W} . Finally, on the curve $\{V_0 = V_{\mathcal{N}_2}(U_0), 0 < U_0 < U_0^*\}$, the trajectories have $V_0' = 0$ and

$$U_0' = -\alpha U_0 + \beta V_{\mathcal{N}_2}(U_0) > -\alpha U_0 + \beta V_{\mathcal{N}_1}(U_0) = 0,$$

meaning that the flux points into \mathcal{W} . Therefore, by Poincaré–Bendixson theorem (Theorem 3.7.1 in [96]), we have that every ω -limit set of a trajectory inside \mathcal{W} is either a fixed point, a periodic orbit, or a heteroclinic orbit between the two fixed points $(0, 0)$ and (U_0^*, V_0^*) . Considering the Dulac function $\phi = -1/V$, we can rule out periodic orbits by applying Dulac’s criterion (Theorem 3.9.2 in [96]). Thus, we obtain the existence of a heteroclinic orbit between $(0, 0)$ and (U_0^*, V_0^*) . Figure 7 illustrates the phase portrait of the system (54) and the heteroclinic orbit between the two equilibria on the left, as well as the heteroclinic orbit and the traveling wave solution of (54) in the wave coordinate ξ on the right.

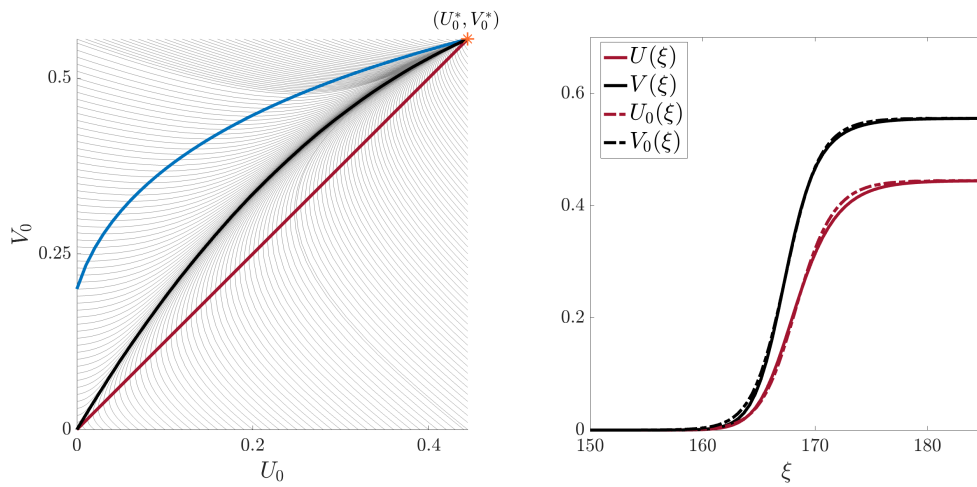


Figure 7: **Large wave speed scaling applied to model (8).** (Left) Phase portrait of system (54). Trajectories are depicted in light grey, while the blue curve represents the V_0 nullcline (55b), the red curve represents the U_0 nullcline (55a), and the black curve represents the heteroclinic connection from the $(0, 0)$ equilibrium to (U_0^*, V_0^*) (orange marker). (Right) Comparison between the traveling wave profile (solid curves) from the model (8) with the corresponding large wave speed approximation (54) (dot-dashed curves) in the coordinate ξ . Logistic growth is assumed in (8), and the parameters (for both plots) are set to $\alpha = 1$, $\beta = 0.8$, $\mu = 0$, and $d = 0.0001$.

The large wave speed scaling has been used extensively in mathematical biology, especially in cancer growth models [98, 106, 107, 138, 139]. It was explicitly used for the total population go-or-grow models in [111, 121] for obtaining an approximation of the traveling wave solution. In particular, in [111], the authors numerically show that for small values of the wave speed, the simulations do not agree, while for larger values of wave speed they observe that the approximation is valid.

8 Discussion

In this article, we have examined the significance of a class of go-or-grow models that are widely employed to describe various biological phenomena, particularly those related to cell

dynamics and cancer progression. What started as a simple review of go-or-grow models quickly became a mathematically involved exposition. Our primary objective has been to provide a comprehensive review of the intriguing mathematical features that characterize this approach, while also highlighting the challenges and open problems that may inspire future mathematical investigations. Despite the biological relevance of these models and their extensive application across various mathematical contexts, a systematic exploration of their mathematical properties and the associated analytical and numerical challenges has been lacking. While we do not claim our analysis is exhaustive, we have endeavored to delve into the diverse array of analytical results available in the literature, examining different mathematical assumptions related to the switching terms of the models and establishing clear connections between the classical FKPP equation and its go-or-grow counterparts.

Beginning with a brief overview of the biological evidence for the emergence of dichotomic dynamics in biological systems, we focused specifically on glioma cell evolution. Research has demonstrated that the progression of this tumor is driven by a proliferation/migration dichotomy, where proliferating cells remain stationary or move slowly, while migrating cells do not proliferate [43, 44]. This serves as the primary biological motivation for our exploration of this class of models. We provided a comprehensive summary of the extensive mathematical literature addressing the go-or-grow dichotomy in glioma progression, spanning from stochastic and discrete approaches to continuous frameworks, with migratory dynamics and population switches influenced by various external and intrinsic factors.

We focused on a specific continuous modeling framework, which we named as the *general go-or-grow model* (4). This model features linear diffusion for the moving population and a characteristic switch between the two populations: migrating cells (u) and proliferating (v) cells. The transition functions $\alpha(\cdot)$ and $\beta(\cdot)$ govern this switching and depend solely on the densities of the populations. Depending on the nature of this dependency, we proposed various specialized versions of the model and reviewed the key papers that have contributed to their analysis. Moreover, we revisited a general existence result for the general model and discussed common scaling techniques that facilitate its analysis, particularly in relation to the classical FKPP equation.

Although these go-or-grow models have been widely employed, they present a range of analytical and numerical challenges associated with the emergence of highly unstable patterns and irregular traveling waves under specific assumptions on the transition functions. While these issues have been observed in different contexts [47, 97], we highlighted and integrated them into a common framework. Singularities arise, driven by an extreme version of the Turing instability, where the diffusion coefficient of the activator is zero. All high frequencies are unstable, leading to oscillations and patterns on fine scales. Of course, this instability has conditions, and if these conditions are not satisfied, then the model is well-behaved.

Focusing on specific analytical properties of go-or-grow models that can be effectively addressed, we extensively reviewed results related to the critical domain problem and the analysis of the existence and minimal speed of traveling wave solutions for the general go-or-grow model and its specialized variants. For the critical domain problem, we revisited classical results concerning the FKPP equation [9, 125] and connected them to findings related to the general go-or-grow model, which show the bifurcation between domain size and the existence of non-trivial steady-state solutions, under specific assumptions about the transition and growth functions. In our examination of traveling wave solutions, we outlined the necessary assumptions that the general go-or-grow model (4) must meet to be classified as a cooperative system. This classification allows us to apply a robust theoretical framework concerning the existence of traveling waves and invasion speed, as established in the literature

[35, 128]. Similar to our analysis of the critical domain size, we establish a connection to the FKPP equation, thereby generalizing previous results to the context of the general go-or-grow model (4) introduced here.

Open Problems While we have reviewed a wide array of analytical and numerical results concerning this special class of mathematical models, several important mathematical questions remain unresolved. One intriguing question that arises from our analysis pertains to the convergence of the fast-transition rate system (12) to system (15) as $\varepsilon \rightarrow 0$, specifically in the context of traveling wave solutions: what assumptions must be satisfied for the limit $\varepsilon \rightarrow 0$ to ensure convergence (in some sense) of (12) to (15)? Furthermore, if (12) meets these necessary conditions, what does the wave speed of (12) converge to in this limit? How does this relate to the minimum wave speed of the corresponding FKPP equation given by (16)?

Similar questions arise when considering large wave speed scaling. Many biological systems can be described by models of the form (4), with specific expressions for the transition functions $\alpha(u, v)$ and $\beta(u, v)$ that may result in noncooperative dynamics. Under what conditions is the existence of traveling waves guaranteed in these noncooperative models, and what is the minimum wave speed associated with them? For cooperative systems, when can we derive an explicit expression for the minimum wave speed, as indicated in (44)?

Additional challenges emerge from the instabilities and patterns discussed in Section 5. How can the autocatalysis condition (22) be formulated for a general model within the go-or-grow family? Is it feasible to develop more sophisticated numerical solvers capable of correctly identifying the sources of the observed instabilities?

These open questions present intriguing opportunities for future research. As we intended to showcase the usefulness of go-or-grow modeling in biology while highlighting interesting mathematical properties, this article is also a warning not to underestimate the monster on a leash.

Acknowledgements 805

We are grateful to the Fields Institute in Toronto, who hosted us for a few weeks in Summer and Fall 2024 to work on this project. RT acknowledges support from a Canadian Graduate Scholarship of the Natural Sciences and Engineering Research Council of Canada (NSERC) and Alberta Innovates Graduate Student Scholarship. MC was supported by the National Group of Mathematical Physics (GNFM-INdAM) through the INdAM–GNFM Project (CUP E53C22001930001) “From kinetic to macroscopic models for tumor-immune system competition”, and by the European Union - NextGenerationEU and the MUR-Italian Ministry of Universities and Research through the project PRIN 2022 PNRR *Mathematical modeling for a Sustainable Circular Economy in Ecosystems* (project code P2022PSMT7, CUP D53D23018960001). MC has been partially supported by the State Research Agency of the Spanish Ministry of Science and FEDER-EU, project PID2022-137228OB-I00 (MICIU/AEI /10.13039/501100011033); by Modeling Nature Research Unit, Grant QUAL21-011 funded by Consejería de Universidad, Investigación e Innovación (Junta de Andalucía). TLS acknowledges support from a National Science Foundation (NSF) grant DMS-2151566. TH is supported through a discovery grant of the Natural Science and Engineering Research Council of Canada (NSERC), RGPIN-2023-04269. 820

Conflict of interest

821

We declare that TH is currently an Editor-in-Chief of the Journal of Mathematical Biology. The research was conducted in the absence of any commercial or financial interests that could be construed as a potential conflict of interest.

822

823

824

Data availability statement

825

Data sharing is not applicable to this article as no data sets were generated or analyzed during the current study.

826

827

A Appendix: Proofs of Lemma 6 and Theorem 7

828

The proofs of Lemma 6 and Theorem 7 primarily require showing that the general go-or-grow model (4) with the assumptions (36b), (40a)–(40b), and (45)–(46) lives inside the general cooperative theory proposed by [35, 77, 128]. In these works, the authors are concerned the n -equation reaction–diffusion system

829

830

831

832

$$\mathbf{w}_t = D\Delta\mathbf{w} + \mathbf{F}(\mathbf{w}), \quad (57)$$

where $\mathbf{w} = (w_1, \dots, w_n)$ and $D = \text{diag}(d_1, \dots, d_n)$, with $d_i \geq 0$ and at least one $d_i \neq 0$. Moreover, we require the following assumptions on the reaction term $\mathbf{F} : \mathbb{R}^n \rightarrow \mathbb{R}^n$:

833

834

- \mathbf{F} is continuous with $\mathbf{F}(\mathbf{0}) = \mathbf{F}(\bar{\mathbf{w}}) = \mathbf{0}$, and there is no ν such that $\mathbf{F}(\nu) = \mathbf{0}$ and $\mathbf{0} < \nu < \bar{\mathbf{w}}$; (58a)

- The system is cooperative, i.e., each component f_i of \mathbf{F} is nondecreasing in all the components of \mathbf{w} , with the possible exception of the i th one; (58b)

- $\mathbf{F}(\mathbf{w})$ is piecewise continuously differentiable in \mathbf{w} for $\mathbf{0} \leq \mathbf{w} \leq \bar{\mathbf{w}}$ and differentiable at $\mathbf{0}$, and the matrix $\mathbf{F}'(\mathbf{0})$ is irreducible with a positive eigenvalue; (58c)

- There exists $a > 0, \sigma > 1$, and $\mathbf{r} > \mathbf{0}$ such that

$$\mathbf{F}(\mathbf{w}) \geq \mathbf{F}'(\mathbf{0})\mathbf{w} - a\|\mathbf{w}\|^\sigma \mathbf{1}, \quad (58d)$$

for all $\mathbf{0} \leq \mathbf{w} \leq \mathbf{r}$, where $\mathbf{1}$ denotes the vector with all entries equal to 1;

- For any $\eta > 0$,

$$\mathbf{F}(\min\{\eta\mathbf{w}(\rho), \mathbf{1}\}) \leq \eta D\mathbf{F}(\mathbf{0})\mathbf{w}(\rho),$$

for all $\rho \in (0, \rho^*]$, where ρ^* is the value of ρ at which $\lambda_+(\rho)/\rho$ attains its infimum.

(58e)

In all the assumptions, the operations are defined component-wise. We show in the following lemma that the general go-or-grow model (4), with the appropriate assumptions, is a special case of the reaction–diffusion equation (57).

835

836

837

Lemma 9. *If the general go-or-grow model (4) satisfies (36b), (40a)–(40b), and (45)–(46), then (4) also satisfies the set of assumptions (58).*

838

839

Proof. Condition (58a), and the first part of condition (58c) are directly satisfied by the assumptions (36b) and (40a). In addition, during the wavefront calculation (Section 7.3), we computed the eigenvalue of the matrix $A = \rho^2 D + \mathbf{F}'(0, 0)$ (42), which for $\rho = 0$ reads

$$\begin{aligned} \lambda_A(0) &= \frac{g(0) - \mu - \alpha(0, 0) - \beta(0, 0)}{2} \\ &\quad + \frac{\sqrt{[g(0) - \mu - \alpha(0, 0) - \beta(0, 0)]^2 + 4[(g(0) - \beta(0, 0))(\mu + \alpha(0, 0)) + \alpha(0, 0)\beta(0, 0)]}}{2} \\ &> \frac{g(0) - \mu - \alpha(0, 0) - \beta(0, 0)}{2} + \frac{\sqrt{[g(0) - \mu - \alpha(0, 0) - \beta(0, 0)]^2}}{2} \geq 0 \end{aligned}$$

completing the requirements for (58c).

For assumption (58b), consider the Jacobian of \mathbf{F} with components

$$\begin{aligned} \mathbf{F}'_{11}(u, v) &= -(\mu - \alpha(u, v)) - \frac{\partial}{\partial u}(\alpha(u, v))u + \frac{\partial}{\partial u}\beta(u, v)v, \\ \mathbf{F}'_{12}(u, v) &= \beta(u, v) - \frac{\partial}{\partial v}\alpha(u, v)u + \frac{\partial}{\partial v}(\beta(u, v))v, \\ \mathbf{F}'_{21}(u, v) &= \alpha(u, v) + \frac{\partial}{\partial u}(\alpha(u, v))u + \frac{\partial}{\partial u}(g(u + v) - \beta(u, v))v, \\ \mathbf{F}'_{22}(u, v) &= (g(u + v) - \beta(u, v)) + \frac{\partial}{\partial v}(g(u + v) - \beta(u, v))v + \frac{\partial}{\partial v}\alpha(u, v)u. \end{aligned}$$

The cooperativity assumption is satisfied by having the off-diagonal terms greater than or equal to zero, which is exactly assumption (40b).

Now, the more technical assumptions (58d) and (58e) need to be satisfied. Considering the first inequality of assumption (46), rearranging terms, and adding $-\mu u$ to both sides yields

$$-(\mu + \alpha(u, v))u + \beta(u, v) \geq -(\mu + \alpha(0, 0))u + \beta(0, 0)v - a|u + v|^\sigma,$$

which is exactly $\mathbf{F}_1(u, v) \geq (\mathbf{F}'_{11}(0, 0), \mathbf{F}'_{12}(0, 0)) \cdot \begin{pmatrix} u \\ v \end{pmatrix} - a|u + v|^\sigma$. For the second component, considering the second inequality of assumption (46) and rearranging terms yields

$$g(u + v)v + \alpha(u, v)u - \beta(u, v)v \geq g(0) - \alpha(0, 0)u + \beta(0, 0)v - a|u + v|^\sigma,$$

which is exactly $\mathbf{F}_2(u, v) \geq (\mathbf{F}'_{21}(0, 0), \mathbf{F}'_{22}(0, 0)) \cdot \begin{pmatrix} u \\ v \end{pmatrix} - a|u + v|^\sigma$. Finally for assumption (58e), we compute

$$\begin{aligned} \mathbf{F}'(0, 0)\nu(\rho) &= \begin{pmatrix} -(\mu - \alpha(0, 0)) & \beta(0, 0) \\ \alpha(0, 0) & g(0) - \beta(0, 0) \end{pmatrix} \begin{pmatrix} \frac{\lambda_A(\rho) - g(0) + \beta(0, 0)}{\alpha(0, 0)} \\ 1 \end{pmatrix} \\ &= \begin{pmatrix} g(0) - \mu\nu_1(\rho) - \lambda_A(\rho) \\ \lambda_A(\rho) \end{pmatrix}. \end{aligned}$$

For the first component, taking the middle inequality of assumption (45), i.e.,

$$-\alpha(\eta\nu_1(\rho), \eta)\nu_1(\rho) + \beta(\eta\nu_1(\rho), \eta) \leq g(0) - \lambda_A(\rho), \quad (59)$$

adding $-\mu\nu_1(\rho)$ to both sides, and multiplying by $\eta > 0$, we get

$$-\alpha(\eta\nu_1(\rho), \eta)\eta - \mu\nu_1(\rho)\eta + \beta(\eta\nu_1(\rho), \eta)\eta \leq (g(0) - \mu\nu_1(\rho) - \lambda_A(\rho))\eta.$$

Notice that this inequality is exactly $\mathbf{F}_1(\eta\nu_1(\rho), \eta) \leq \eta(\mathbf{F}'_{11}(0, 0), \mathbf{F}'_{12}(0, 0)) \cdot (\eta\nu_1(\rho), \eta)^T$. For the second component, we consider the first inequality of assumption (45), i.e.,

$$g(\eta + \eta\nu_1(\rho)) \leq -\alpha(\eta\nu_1(\rho), \eta) + \beta(\eta\nu_1(\rho), \eta) + \lambda_A(\rho).$$

Rearranging terms and multiplying by η , we get

$$\alpha(\eta\nu_1(\rho), \eta)\eta - \beta(\eta\nu_1(\rho), \eta)\eta + g(\eta + \eta\nu_1(\rho))\eta \leq \lambda_A(\rho)\eta,$$

which is $\mathbf{F}_2(\eta\nu_1(\rho), \eta) \leq \eta(\mathbf{F}'_{21}(0, 0), \mathbf{F}'_{22}(0, 0)) \cdot (\eta\nu_1(\rho), \eta)^T$.

Therefore, if (4) satisfies (36b), (40a)–(40b), and (45)–(46), then (4) also satisfies (58). \square

Since the general go-org-grow model (4) satisfies the general conditions (58), we can apply the following lemma to obtain information on the spreading speed.

Lemma 10 ([35, 77, 128]). *Let \mathbf{F} satisfy (58a)–(58c), and consider the initial condition $\phi \in \mathcal{C}_{\bar{\mathbf{w}}} = \{(\phi_1, \dots, \phi_n) \in C(\mathbb{R}; \mathbb{R}^n) : 0 \leq \phi_i(z) \leq \bar{w}_i \forall z \in \mathbb{R}\}$ and $\mathbf{w}(t, x; \phi)$ be the unique solution of (57) through ϕ . Then there exists a real number $0 < \tilde{c} \leq \bar{c}$, where*

$$\bar{c} = \inf_{\mu > 0} \Phi(\mu), \quad (60)$$

such that the following statements are valid:

- (i) $\Phi(\mu) = \frac{\lambda_A(\mu)}{\mu}$ is decreasing as μ nears 0 and tends to infinity as $\mu \rightarrow 0$; $\Phi'(\mu)$ changes sign at most once in $(0, \infty)$ and $\lim_{\mu \rightarrow \infty} \Phi(\mu) = +\infty$;
- (ii) If ϕ has compact support, then $\lim_{\substack{t \rightarrow \infty \\ |x| \geq ct}} \mathbf{w}(t, x; \phi) = 0$, for all $c > \tilde{c}$;
- (iii) For any $c \in (0, \tilde{c})$ and any vector $\mathbf{r} > \mathbf{0}$, there is a positive number R_r such that for any $\phi \in \mathcal{C}_{\bar{\mathbf{w}}}$ with $\phi \leq \mathbf{r}$ on an interval of length $2R_r$, it holds that $\lim_{\substack{t \rightarrow \infty \\ |x| \leq ct}} \mathbf{w}(t, x; \phi) = \bar{\mathbf{w}}$;
- (iv) If, in addition, $\mathbf{F}(\min\{\rho\nu(\mu^*), \mathbf{1}\}) \leq \rho\mathbf{F}'(\mathbf{0})\nu(\mu)$, for all $\rho > 0$, then $\tilde{c} = \bar{c}$, where μ^* is the value of μ at which $\Phi(\mu)$ attains its infimum.

Finally, we use the following theorem to prove the existence of traveling wave solutions.

Theorem 11 (Theorem 3.1 in [35]). *Assume the set of assumptions (58) hold, then for each $c \geq \bar{c}$, system (57) has a nondecreasing wavefront $W(x + ct)$ connecting $\mathbf{0}$ and $\bar{\mathbf{w}}$; while for any $c \in (0, \bar{c})$, there is no wavefront $W(x + ct)$ connecting $\mathbf{0}$ and $\bar{\mathbf{w}}$*

Applying Lemma 10 and Theorem 11 to the general go-org-grow model (4), with assumptions (36b), (40a)–(40b), and (45)–(46), proves Lemma 6 and Theorem 7.

References

879

1. Alfonso, J. *et al.* The biology and mathematical modelling of glioma invasion: A review. *Journal of the Royal Society Interface* **14**, 20170490. doi:[10.1098/rsif.2017.0490](https://doi.org/10.1098/rsif.2017.0490) (2017).
880
881
882
2. Alfonso, J. C. L. *et al.* Why one-size-fits-all vaso-modulatory interventions fail to control glioma invasion: in silico insights. *Scientific reports* **6**, 37283. doi:[10.1038/srep37283](https://doi.org/10.1038/srep37283) (2016).
883
884
885
3. Alsisi, A., Eftimie, R. & Trucu, D. Non-local multiscale approach for the impact of go or grow hypothesis on tumour-viruses interactions. *Mathematical Biosciences and Engineering* **18**, 5252–5284. doi:[10.3934/mbe.2021267](https://doi.org/10.3934/mbe.2021267) (2021).
886
887
888
4. Ayuso, J. M. *et al.* Glioblastoma on a microfluidic chip: Generating pseudopalisades and enhancing aggressiveness through blood vessel obstruction events. *Neuro-oncology* **19**, 503–513. doi:[10.1093/neuonc/now230](https://doi.org/10.1093/neuonc/now230) (2017).
889
890
891
5. Berens, M. E. & Giese, A. “... those left behind.” Biology and oncology of invasive glioma cells. *Neoplasia* **1**, 208–219. doi:[10.1038/sj.neo.7900034](https://doi.org/10.1038/sj.neo.7900034) (1999).
892
893
6. Billingham, J. & Needham, D. J. The development of travelling waves in quadratic and cubic autocatalysis with unequal diffusion rates. I. Permanent form travelling waves. *Philosophical Transactions of the Royal Society of London. Series A: Physical and Engineering Sciences* **334**, 1–24. doi:[10.1098/rsta.1991.0001](https://doi.org/10.1098/rsta.1991.0001) (1991).
894
895
896
897
7. Böttger, K., Hatzikirou, H., Chauviere, A. & Deutsch, A. Investigation of the migration/proliferation dichotomy and its impact on avascular glioma invasion. *Mathematical Modelling of Natural Phenomena* **7**, 105–135. doi:[10.1051/mmnp/20127106](https://doi.org/10.1051/mmnp/20127106) (2012).
898
899
900
8. Böttger, K. *et al.* An Emerging Allee Effect Is Critical For Tumor Initiation and Persistence. *PLOS Computational Biology* **11**, e1004366. doi:[10.1371/journal.pcbi.1004366](https://doi.org/10.1371/journal.pcbi.1004366) (2015).
901
902
903
9. Britton, N. *Reaction–Diffusion Equations and Their Applications to Biology* (Academic Press, London, 1986).
904
905
10. Burger, M., Friele, P. & Pietschmann, J.-F. On a reaction-cross-diffusion system modeling the growth of glioblastoma. *SIAM Journal on Applied Mathematics* **80**, 160–182. doi:[10.1137/18M1194559](https://doi.org/10.1137/18M1194559) (2020).
906
907
908
11. Canosa, J. On a nonlinear diffusion equation describing population growth. *IBM Journal of Research and Development* **17**, 307–313. doi:[10.1147/rd.174.0307](https://doi.org/10.1147/rd.174.0307) (1973).
909
910
12. Capasso, V. & Maddalena, L. Convergence to equilibrium states for a reaction-diffusion system modelling the spatial spread of a class of bacterial and viral diseases. *Journal of Mathematical Biology* **13**, 173–184. doi:[10.1007/BF00275212](https://doi.org/10.1007/BF00275212) (1981).
911
912
913
13. Chauviere, A., Preziosi, L. & Byrne, H. A model of cell migration within the extracellular matrix based on a phenotypic switching mechanism. *Mathematical Medicine and Biology* **27**, 255–281. doi:[10.1093/imammb/dqp021](https://doi.org/10.1093/imammb/dqp021) (2010).
914
915
916
14. Chen, C. & Wang, H. Steady-state bifurcation and spike pattern in the Klausmeier-Gray-Scott model with non-diffusive plants. *Discrete and Continuous Dynamical Systems - B* **29**, 4973–4999. doi:[10.3934/dcdsb.2024074](https://doi.org/10.3934/dcdsb.2024074) (2024).
917
918
919
15. Chuan, L. H., Tsujikawa, T. & Yagi, A. Asymptotic behavior of solutions for forest kinematic model. *Funkcialaj Ekvacioj* **49**, 427–449. doi:[10.1619/fesi.49.427](https://doi.org/10.1619/fesi.49.427) (2006).
920
921

16. Ciocanel, M.-V., Sandstede, B., Jeschonek, S. P. & Mowry, K. L. Modeling microtubule-based transport and anchoring of mRNA. *SIAM Journal on Applied Dynamical Systems* **17**, 2855–2881. doi:[10.1137/18M1186083](https://doi.org/10.1137/18M1186083) (2018). 922–924
17. Cochet-Escartin, O. *et al.* Hypoxia triggers collective aerotactic migration in *Dicystostelium discoideum*. *eLife* **10**, e64731. doi:[10.7554/eLife.64731](https://doi.org/10.7554/eLife.64731) (2021). 925–926
18. Colombo, M. C. *et al.* Towards the personalized treatment of glioblastoma: Integrating patient-specific clinical data in a continuous mechanical model. *PLOS ONE* **10**, e0132887. doi:[10.1371/journal.pone.0132887](https://doi.org/10.1371/journal.pone.0132887) (2015). 927–929
19. Conte, M., Gerardo-Giorda, L. & Groppi, M. Glioma invasion and its interplay with nervous tissue and therapy: A multiscale model. *Journal of Theoretical Biology* **486**, 110088. doi:[10.1016/j.jtbi.2019.110088](https://doi.org/10.1016/j.jtbi.2019.110088) (2020). 930–932
20. Conte, M., Casas-Tinto, S. & Soler, J. Modeling invasion patterns in the glioblastoma battlefield. *PLOS Computational Biology* **17**, e1008632. doi:[10.1371/journal.pcbi.1008632](https://doi.org/10.1371/journal.pcbi.1008632) (Jan. 2021). 933–935
21. Conte, M., Dzierma, Y., Knobe, S. & Surulescu, C. Mathematical modeling of glioma invasion and therapy approaches via kinetic theory of active particles. *Mathematical Models and Methods in Applied Sciences* **33**, 1009–1051. doi:[10.1142/S0218202523500227](https://doi.org/10.1142/S0218202523500227) (2023). 936–939
22. Conte, M. & Surulescu, C. Mathematical modeling of glioma invasion: Acid- and vasculature mediated go-or-grow dichotomy and the influence of tissue anisotropy. *Applied Mathematics and Computation* **407**, 126305. doi:[10.1016/j.amc.2021.126305](https://doi.org/10.1016/j.amc.2021.126305) (2021). 940–942
23. Crossley, R. M., Painter, K. J., Lorenzi, T., Maini, P. K. & Baker, R. E. Phenotypic switching mechanisms determine the structure of cell migration into extracellular matrix under the ‘go-or-grow’ hypothesis. *Mathematical Biosciences* **374**, 109240. doi:[10.1016/j.mbs.2024.109240](https://doi.org/10.1016/j.mbs.2024.109240) (2024). 943–946
24. Cuddapah, V. A., Robel, S., Watkins, S. & Sontheimer, H. A neurocentric perspective on glioma invasion. *Nature Reviews Neuroscience* **15**, 455–465. doi:[10.1038/nrn3765](https://doi.org/10.1038/nrn3765) (2014). 947–949
25. Curtin, L., Hawkins-Daarud, A., Van Der Zee, K. G., Swanson, K. R. & Owen, M. R. Speed switch in glioblastoma growth rate due to enhanced hypoxia-induced migration. *Bulletin of Mathematical Biology* **82**, 43. doi:[10.1007/s11538-020-00718-x](https://doi.org/10.1007/s11538-020-00718-x) (2020). 950–952
26. Curtin, L. *et al.* A mechanistic investigation into ischemia-driven distal recurrence of glioblastoma. *Bulletin of Mathematical Biology* **82**, 143. doi:[10.1007/s11538-020-00814-y](https://doi.org/10.1007/s11538-020-00814-y) (2020). 953–955
27. de Vries, G., Hillen, T., Lewis, M., Müller, J. & Schönfish, B. *A Course in Mathematical Biology: Quantitative Modeling with Mathematical and Computational Methods* (SIAM, Philadelphia, PA, 2006). 956–958
28. Dunbar, S. R. Traveling wave solutions of diffusive Lotka–Volterra equations: A heteroclinic connection in R^4 . *Transactions of the American Mathematical Society* **286**, 557–594. doi:[10.2307/1999810](https://doi.org/10.2307/1999810) (1984). 959–961
29. Dunbar, S. R. Traveling waves in diffusive predator–prey equations: Periodic orbits and point-to-periodic heteroclinic orbits. *SIAM Journal on Applied Mathematics* **46**, 1057–1078. doi:[10.1137/0146063](https://doi.org/10.1137/0146063) (1986). 962–964

30. Dunbar, S. R. Travelling wave solutions of diffusive Lotka–Volterra equations. *Journal of Mathematical Biology* **17**, 11–32. doi:[10.1007/BF00276112](https://doi.org/10.1007/BF00276112) (1983). 965 966
31. Engwer, C., Hillen, T., Knappitsch, M. & Surulescu, C. Glioma follow white matter tracts: a multiscale DTI-based model. *Journal of Mathematical Biology* **71**, 551–582. doi:[10.1007/s00285-014-0822-7](https://doi.org/10.1007/s00285-014-0822-7) (2015). 967 968 969
32. Engwer, C., Hunt, A. & Surulescu, C. Effective equations for anisotropic glioma spread with proliferation: A multiscale approach and comparisons with previous settings. *Mathematical medicine and biology: a journal of the IMA* **33**, 435–459. doi:[10.1093/imammb/dqv030](https://doi.org/10.1093/imammb/dqv030) (2016). 970 971 972 973
33. Engwer, C., Knappitsch, M. & Surulescu, C. A multiscale model for glioma spread including cell-tissue interactions and proliferation. *Mathematical Biosciences & Engineering* **13**, 443–460. doi:[10.3934/mbe.2015011](https://doi.org/10.3934/mbe.2015011) (2015). 974 975 976
34. Falcó, C., Crossley, R. M. & Baker, R. E. Travelling waves in a minimal go-or-grow model of cell invasion. *Applied Mathematics Letters* **158**, 109209. doi:[10.1016/j.aml.2024.109209](https://doi.org/10.1016/j.aml.2024.109209) (2024). 977 978 979
35. Fang, J. & Zhao, X.-Q. Monotone wavefronts for partially degenerate reaction-diffusion systems. *Journal of Dynamics and Differential Equations* **21**, 663–680. doi:[10.1007/s10884-009-9152-7](https://doi.org/10.1007/s10884-009-9152-7) (2009). 980 981 982
36. Farin, A. *et al.* Transplanted glioma cells migrate and proliferate on host brain vasculature: A dynamic analysis. *Glia* **53**, 799–808. doi:[10.1002/glia.20334](https://doi.org/10.1002/glia.20334) (2006). 983 984
37. Fedotov, S. & Iomin, A. Probabilistic approach to a proliferation and migration dichotomy in tumor cell invasion. *Physical Review E* **77**, 031911. doi:[10.1103/PhysRevE.77.031911](https://doi.org/10.1103/PhysRevE.77.031911) (2008). 985 986 987
38. Fedotov, S. & Iomin, A. Migration and proliferation dichotomy in tumor-cell invasion. *Physical Review Letters* **98**, 118101. doi:[10.1103/PhysRevLett.98.118101](https://doi.org/10.1103/PhysRevLett.98.118101) (2007). 988 989
39. Finlayson, A. & Merkin, J. Travelling waves in an open quadratic autocatalytic chemical system. *Journal of Mathematical Chemistry* **21**, 305–321. doi:[10.1023/A:1019134822110](https://doi.org/10.1023/A:1019134822110) (1997). 990 991 992
40. Garay, T. *et al.* Cell migration or cytokinesis and proliferation? – Revisiting the “go or grow” hypothesis in cancer cells in vitro. *Experimental Cell Research* **319**, 3094–3103. doi:[10.1016/j.yexcr.2013.08.018](https://doi.org/10.1016/j.yexcr.2013.08.018) (2013). 993 994 995
41. Gerlee, P. & Nelander, S. The impact of phenotypic switching on glioblastoma growth and invasion. *PLOS Computational Biology* **8**, e1002556. doi:[10.1371/journal.pcbi.1002556](https://doi.org/10.1371/journal.pcbi.1002556) (2012). 996 997 998
42. Gerlee, P. & Nelander, S. Travelling wave analysis of a mathematical model of glioblastoma growth. *Mathematical Biosciences* **276**, 75–81. doi:[10.1016/j.mbs.2016.03.004](https://doi.org/10.1016/j.mbs.2016.03.004) (2016). 999 1000 1001
43. Giese, A., Bjerkvig, R., Berens, M. & Westphal, M. Cost of migration: Invasion of malignant gliomas and implications for treatment. *Journal of Clinical Oncology* **21**, 1624–1636. doi:[10.1200/JCO.2003.05.063](https://doi.org/10.1200/JCO.2003.05.063) (2003). 1002 1003 1004
44. Giese, A. *et al.* Dichotomy of astrocytoma migration and proliferation. *International Journal of Cancer* **67**, 275–282. doi:[10.1002/\(SICI\)1097-0215\(19960717\)67:2<275::AID-IJC20>3.0.CO;2-9](https://doi.org/10.1002/(SICI)1097-0215(19960717)67:2<275::AID-IJC20>3.0.CO;2-9) (1996). 1005 1006 1007

45. Godlewski, J., Bronisz, A., Nowicki, M. O., Chiocca, E. A. & Lawler, S. microRNA-451: 1008
A conditional switch controlling glioma cell proliferation and migration. *Cell Cycle* **9**, 1009
2814–2820. doi:10.4161/cc.9.14.12248 (2010). 1010
46. Haderer, K. & Lewis, M. Spatial dynamics of the diffusive logistic equation with a 1011
sedentary compartment. *Canadian Applied Mathematics Quarterly* **10**, 473–498 (2002). 1012
47. Härtling, S. & Marciniak-Czochra, A. Spike patterns in a reaction–diffusion ODE model 1013
with Turing instability. *Mathematical Methods in the Applied Sciences* **37**, 1377–1391. 1014
doi:10.1002/mma.2899 (2014). 1015
48. Hatzikirou, H., Basanta, D., Simon, M., Schaller, K. & Deutsch, A. “Go or grow”: The 1016
key to the emergence of invasion in tumour progression? *Mathematical Medicine and* 1017
Biology: A Journal of the IMA **29**, 49–65. doi:10.1093/imamb/dqq011 (2012). 1018
49. Hatzikirou, H., Deutsch, A., Schaller, C., Simon, M. & Swanson, K. Mathematical 1019
modelling of glioblastoma tumour development: A review. *Mathematical Models and* 1020
Methods in Applied Sciences **15**, 1779–1794. doi:10.1142/S0218202505000960 (2005). 1021
50. Hillen, T. *Elements of Applied Functional Analysis* (American Mathematical Society 1022
Open Math Notes, Providence, RI, 2023). 1023
51. Hillen, T., Loy, N., Painter, K. & Thiessen, R. Modelling microtubule driven invasion of 1024
glioma. *Journal of Mathematical Biology* **88**, 1–34. doi:10.1007/s00285-023-02025-0 1025
(2024). 1026
52. Hoek, K. S. *et al.* In vivo switching of human melanoma cells between proliferative and 1027
invasive states. *Cancer Research* **68**, 650–656. doi:10.1158/0008-5472.CAN-07-2491 1028
(2008). 1029
53. Hormuth, D. *et al.* Opportunities for improving brain cancer treatment outcomes through 1030
imaging-based mathematical modeling of the delivery of radiotherapy and immunother- 1031
apy. *Advanced Drug Delivery Reviews* **187**, 114367. doi:10.1016/j.addr.2022.114367 1032
(2022). 1033
54. Hou, L. C., Veeravagu, A., Hsu, A. R. & Victor, C. Recurrent glioblastoma multiforme: 1034
A review of natural history and management options. *Neurosurgical Focus* **20**, E3. 1035
doi:10.3171/foc.2006.20.4.2 (2006). 1036
55. Hsu, C.-H., Yang, C.-R., Yang, T.-H. & Yang, T.-S. Existence of traveling wave solutions 1037
for diffusive predator–prey type systems. *Journal of Differential Equations* **252**, 3040– 1038
3075. doi:10.1016/j.jde.2011.11.008 (2012). 1039
56. Huang, J., Lu, G. & Ruan, S. Existence of traveling wave solutions in a diffusive 1040
predator-prey model. *Journal of Mathematical Biology* **46**, 132–152. doi:10.1007 / 1041
s00285-002-0171-9 (2003). 1042
57. Huang, Q., Jin, Y. & Lewis, M. A. R_0 analysis of a benthic-drift model for a stream 1043
population. *SIAM Journal on Applied Dynamical Systems* **15**, 287–321. doi:10.1137 / 1044
15M1014486 (2016). 1045
58. Huang, Q., Wang, H. & Lewis, M. A. A hybrid continuous/discrete-time model for 1046
invasion dynamics of zebra mussels in rivers. *SIAM Journal on Applied Mathematics* 1047
77, 854–880. doi:10.1137/16M1057826 (2017). 1048
59. Huang, W. A geometric approach in the study of traveling waves for some classes of 1049
non-monotone reaction–diffusion systems. *Journal of Differential Equations* **260**, 2190– 1050
2224. doi:10.1016/j.jde.2015.09.060 (2016). 1051

60. Huang, W. Traveling wave solutions for a class of predator–prey systems. *Journal of Dynamics and Differential Equations* **24**, 633–644. doi:[10.1007/s10884-012-9255-4](https://doi.org/10.1007/s10884-012-9255-4) (2012).
61. Hunt, A. & Surulescu, C. A multiscale modeling approach to glioma invasion with therapy. *Vietnam Journal of Mathematics* **45**, 221–240. doi:[10.1007/s10013-016-0223-x](https://doi.org/10.1007/s10013-016-0223-x) (2017).
62. Jbabdi, S. *et al.* Simulation of anisotropic growth of low-grade gliomas using diffusion tensor imaging. *Magnetic Resonance in Medicine* **54**, 616–624. doi:[10.1002/mrm.20625](https://doi.org/10.1002/mrm.20625) (2005).
63. Jin, Y. & Zhao, X.-Q. The spatial dynamics of a zebra mussel model in river environments. *Discrete and Continuous Dynamical Systems - B* **26**, 1991–2010. doi:[10.3934/dcdsb.2020362](https://doi.org/10.3934/dcdsb.2020362) (2021).
64. Jørgensen, A. C. S. *et al.* Data-driven spatio-temporal modelling of glioblastoma. *Royal Society Open Science* **10**, 221444. doi:[10.1098/rsos.221444](https://doi.org/10.1098/rsos.221444) (2023).
65. Kim, Y., Lawler, S., Nowicki, M. O., Chiocca, E. A. & Friedman, A. A mathematical model for pattern formation of glioma cells outside the tumor spheroid core. *Journal of theoretical biology* **260**, 359–371. doi:[10.1016/j.jtbi.2009.06.025](https://doi.org/10.1016/j.jtbi.2009.06.025) (2009).
66. Kim, Y. & Roh, S. A hybrid model for cell proliferation and migration in glioblastoma. *Discrete and Continuous Dynamical Systems-B* **18**, 969–1015. doi:[10.3934/dcdsb.2013.18.969](https://doi.org/10.3934/dcdsb.2013.18.969) (2013).
67. Kuznetsov, M. & Kolobov, A. Investigation of solid tumor progression with account of proliferation/migration dichotomy via Darwinian mathematical model. *Journal of Mathematical Biology* **80**, 601–626. doi:[10.1007/s00285-019-01434-4](https://doi.org/10.1007/s00285-019-01434-4) (2020).
68. Kuznetsov, Y. A., Antonovsky, M. Y., Biktashev, V. N. & Aponina, E. A. A cross-diffusion model of forest boundary dynamics. *Journal of Mathematical Biology* **32**, 219–232. doi:[10.1007/BF00163879](https://doi.org/10.1007/BF00163879) (1994).
69. Lam, K.-Y., Wang, X. & Zhang, T. Traveling waves for a class of diffusive disease-transmission models with network structures. *SIAM Journal on Mathematical Analysis* **50**, 5719–5748. doi:[10.1137/17M114425](https://doi.org/10.1137/17M114425) (2018).
70. Landman, K. A., Cai, A. Q. & Hughes, B. D. Travelling waves of attached and detached cells in a wound-healing cell migration assay. *Bulletin of Mathematical Biology* **69**, 2119–2138. doi:[10.1007/s11538-007-9206-0](https://doi.org/10.1007/s11538-007-9206-0) (2007).
71. Levin, S. & Okubo, A. *Diffusion and Ecological Problems: Modern Perspectives* 2nd. doi:[10.1007/978-1-4757-4978-6](https://doi.org/10.1007/978-1-4757-4978-6) (Springer-Verlag, New York, 2002).
72. Lewis, M. A., Schmitz, G., Kareiva, P. & Trevors, J. T. Models to examine containment and spread of genetically engineered microbes. *Molecular Ecology* **5**, 165–175. doi:[10.1046/j.1365-294X.1996.00228.x](https://doi.org/10.1046/j.1365-294X.1996.00228.x) (1996).
73. Lewis, M., Li, B. & Weinberger, H. Spreading Speed and Linear Determinacy for two-species competition model. *Journal of Mathematical Biology* **45**, 219–312. doi:[10.1007/s002850200144](https://doi.org/10.1007/s002850200144) (2002).
74. Lewis, M. & Schmitz, G. Biological invasion of an organism with separate mobile and stationary states: Modeling and analysis. *Forma* **11**, 1–25 (1996).

75. Li, W.-T. & Wu, S.-L. Traveling waves in a diffusive predator–prey model with Holling type-III functional response. *Chaos, Solitons & Fractals* **37**, 476–486. doi:[10.1016/j.chaos.2006.09.039](https://doi.org/10.1016/j.chaos.2006.09.039) (2008). 1094–1096
76. Liang, X., Zhang, L. & Zhao, X.-Q. The principal eigenvalue for degenerate periodic reaction-diffusion systems. *SIAM Journal on Mathematical Analysis* **49**, 3603–3636. doi:[10.1137/16M1108832](https://doi.org/10.1137/16M1108832) (2017). 1097–1099
77. Liang, X. & Zhao, X.-Q. Asymptotic speeds of spread and traveling waves for monotone semiflows with applications. *Communications on Pure and Applied Mathematics* **60**, 1–40. doi:[10.1002/cpa.20154](https://doi.org/10.1002/cpa.20154) (2007). 1100–1102
78. Lin, X., Weng, P. & Wu, C. Traveling wave solutions for a predator–prey system with sigmoidal response function. *Journal of Dynamics and Differential Equations* **23**, 903–921. doi:[10.1007/s10884-011-9220-7](https://doi.org/10.1007/s10884-011-9220-7) (2011). 1103–1105
79. Lutscher, F., Lewis, M. A. & McCauley, E. Effects of heterogeneity on spread and persistence in rivers. *Bulletin of Mathematical Biology* **68**, 2129–2160. doi:[10.1007/s11538-006-9100-1](https://doi.org/10.1007/s11538-006-9100-1) (2006). 1106–1108
80. Lutscher, F., McCauley, E. & Lewis, M. A. Spatial patterns and coexistence mechanisms in systems with unidirectional flow. *Theoretical Population Biology* **71**, 267–277. doi:[10.1016/j.tpb.2006.11.006](https://doi.org/10.1016/j.tpb.2006.11.006) (2007). 1109–1111
81. Lutscher, F. & Seo, G. The effect of temporal variability on persistence conditions in rivers. *Journal of Theoretical Biology* **283**, 53–59. doi:[10.1016/j.jtbi.2011.05.032](https://doi.org/10.1016/j.jtbi.2011.05.032) (2011). 1112–1114
82. Marciniak-Czochra, A. *Reaction-diffusion-ODE models of pattern formation in Evolutionary Equations with Applications in Natural Sciences* (eds Banasiak, J. & Mokhtar-Kharroubi, M.) 387–438 (Springer International Publishing, Cham, 2015). doi:[10.1007/978-3-319-11322-7_8](https://doi.org/10.1007/978-3-319-11322-7_8). 1115–1118
83. Martínez-González, A., Calvo, G. F., Pérez Romasanta, L. A. & Pérez-García, V. M. Hypoxic cell waves around necrotic cores in glioblastoma: a biomathematical model and its therapeutic implications. *Bulletin of Mathematical Biology* **74**, 2875–2896. doi:[10.1007/s11538-012-9786-1](https://doi.org/10.1007/s11538-012-9786-1) (2012). 1119–1122
84. Martirosyan, N. L. *et al.* Mathematically modeling the biological properties of gliomas: A review. *Mathematical Biosciences and Engineering* **12**, 879–905. doi:[10.3934/mbe.2015.12.879](https://doi.org/10.3934/mbe.2015.12.879) (2015). 1123–1125
85. Merkin, J. & Sadiq, M. A. The propagation of travelling waves in an open cubic autocatalytic chemical system. *IMA Journal of Applied Mathematics* **57**, 273–309. doi:[10.1093/imamat/57.3.273](https://doi.org/10.1093/imamat/57.3.273) (1996). 1126–1128
86. Merkin, J. H., Petrov, V., Scott, S. K. & Showalter, K. Wave-induced chemical chaos. *Physical Review Letters* **76**, 546–549. doi:[10.1103/PhysRevLett.76.546](https://doi.org/10.1103/PhysRevLett.76.546) (1996). 1129–1130
87. Murray, J. D. *Mathematical Biology: I. An Introduction* doi:[10.1007/b98868](https://doi.org/10.1007/b98868) (Springer, New York, NY, 2002). 1131–1132
88. Murray, J. D. *Mathematical Biology: II. Spatial Models and Biomedical Applications* doi:[10.1007/b98869](https://doi.org/10.1007/b98869) (Springer, New York, NY, 2003). 1133–1134
89. Odde, D. J. *Glioblastoma cell invasion: Go? Grow? Yes* 2023. doi:[10.1093/neuonc/noad178](https://doi.org/10.1093/neuonc/noad178). 1135–1136

90. Osswald, M. *et al.* Brain tumour cells interconnect to a functional and resistant network. *Nature* **528**, 93–98. doi:[10.1038/nature16071](https://doi.org/10.1038/nature16071) (2015). 1137–1138
91. Ostrom, Q. T. *et al.* The epidemiology of glioma in adults: a “state of the science” review. *Neuro-oncology* **16**, 896–913. doi:[10.1093/neuonc/nou087](https://doi.org/10.1093/neuonc/nou087) (2014). 1139–1140
92. Pachepsky, E., Lutscher, F., Nisbet, R. & Lewis, M. Persistence, spread and the drift paradox. *Theoretical Population Biology* **67**, 61–73. doi:[10.1016/j.tpb.2004.09.001](https://doi.org/10.1016/j.tpb.2004.09.001) (2005). 1141–1143
93. Painter, K. & Hillen, T. Mathematical modelling of glioma growth: the use of diffusion tensor imaging (DTI) data to predict the anisotropic pathways of cancer invasion. *Journal of Theoretical Biology* **323**, 25–39. doi:[10.1016/j.jtbi.2013.01.014](https://doi.org/10.1016/j.jtbi.2013.01.014) (2013). 1144–1146
94. Pardo, R., Martínez-González, A. & Pérez-García, V. M. Nonlinear ghost waves accelerate the progression of high-grade brain tumors. *Communications in Nonlinear Science and Numerical Simulation* **39**, 360–380. doi:[10.1016/j.cnsns.2016.03.014](https://doi.org/10.1016/j.cnsns.2016.03.014) (2016). 1147–1149
95. Patra, P. & Klumpp, S. Role of bacterial persistence in spatial population expansion. *Physical Review E* **104**, 034401. doi:[10.1103/PhysRevE.104.034401](https://doi.org/10.1103/PhysRevE.104.034401) (2021). 1150–1151
96. Perko, L. *Differential equations and dynamical systems* (Springer Science & Business Media, 2013). 1152–1153
97. Pham, K. *et al.* Density-dependent quiescence in glioma invasion: instability in a simple reaction–diffusion model for the migration/proliferation dichotomy. *Journal of Biological Dynamics* **6**, 54–71. doi:[10.1080/17513758.2011.590610](https://doi.org/10.1080/17513758.2011.590610) (2012). 1154–1156
98. Quinn, T. & Sinkala, Z. Dynamics of prostate cancer stem cells with diffusion and organism response. *BioSystems* **96**, 69–79. doi:[10.1016/j.biosystems.2008.11.010](https://doi.org/10.1016/j.biosystems.2008.11.010) (2009). 1157–1159
99. Ratliff, M. *et al.* Individual glioblastoma cells harbor both proliferative and invasive capabilities during tumor progression. *Neuro-oncology* **25**, 2150–2162. doi:[10.1093/neuonc/noad109](https://doi.org/10.1093/neuonc/noad109) (2023). 1160–1162
100. Robinson, J. *Infinite-Dimensional Dynamical Systems* (Cambridge University Press, Cambridge, 2001). 1163–1164
101. Rothe, F. *Global Solutions of Reaction-Diffusion Systems* (Springer, Berlin, 1984). 1165
102. Sadiq, M. A. & Merkin, J. H. Travelling waves in an open cubic autocatalytic system. *Journal of Mathematical Chemistry* **20**, 213–233. doi:[10.1007/BF01165344](https://doi.org/10.1007/BF01165344) (1996). 1166–1167
103. Saut, O., Lagaert, J.-B., Colin, T. & Fathallah-Shaykh, H. M. A multilayer grow-or-go model for GBM: Effects of invasive cells and anti-angiogenesis on growth. *Bulletin of Mathematical Biology* **76**, 2306–2333. doi:[10.1007/s11538-014-0007-y](https://doi.org/10.1007/s11538-014-0007-y) (2014). 1168–1170
104. Scribner, E. & Fathallah-Shaykh, H. M. Single cell mathematical model successfully replicates key features of GBM: go-or-grow is not necessary. *PLOS One* **12**, e0169434. doi:[10.1371/journal.pone.0169434](https://doi.org/10.1371/journal.pone.0169434) (2017). 1171–1173
105. Sewalt, L. & Doelman, A. Spatially periodic multipulse patterns in a generalized Klausmeier–Gray–Scott model. *SIAM Journal on Applied Dynamical Systems* **16**, 1113–1163. doi:[10.1137/16M1078756](https://doi.org/10.1137/16M1078756) (2017). 1175–1176
106. Sherratt, J. A. Wavefront propagation in a competition equation with a new motility term modelling contact inhibition between cell populations. *Proceedings of the Royal Society of London. Series A: Mathematical, Physical and Engineering Sciences* **456**, 2365–2386. doi:[10.1098/rspa.2000.0616](https://doi.org/10.1098/rspa.2000.0616) (2000). 1177–1180

107. Sherratt, J. A. & Chaplain, M. A. A new mathematical model for avascular tumour growth. *Journal of Mathematical Biology* **43**, 291–312. doi:10.1007/s002850100088 (2001).
108. Smoller, J. *Shock Waves and Reaction–Diffusion Equations* doi:10.1007/978-1-4612-0873-0 (Springer-Verlag, New York, 1983).
109. Stein, A. M., Demuth, T., Mobley, D., Berens, M. & Sander, L. M. A mathematical model of glioblastoma tumor spheroid invasion in a three-dimensional in vitro experiment. *Biophysical Journal* **92**, 356–365. doi:0.1529/biophysj.106.093468 (2007).
110. Stein, S., Zhao, R., Haeno, H., Vivanco, I. & Michor, F. Mathematical modeling identifies optimum lapatinib dosing schedules for the treatment of glioblastoma patients. *PLOS Computational Biology* **14**, e1005924. doi:10.1371/journal.pcbi.1005924 (2018).
111. Stepien, T. L., Rutter, E. M. & Kuang, Y. Traveling waves of a go-or-grow model of glioma growth. *SIAM Journal on Applied Mathematics* **78**, 1778–1801. doi:10.1137/17M1146257 (2018).
112. Stinner, C., Surulescu, C. & Uatay, A. Global existence for a go-or-grow multiscale model for tumor invasion with therapy. *Mathematical Models and Methods in Applied Sciences* **26**, 2163–2201. doi:10.1142/S021820251640011X (2016).
113. Swan, A., Hillen, T., Bowman, J. C. & Murtha, A. D. A patient-specific anisotropic diffusion model for brain tumour spread. *Bulletin of mathematical biology* **80**, 1259–1291. doi:10.1007/s11538-017-0271-8 (2018).
114. Swanson, K., Rostomily, R. & Alvord, E. A mathematical modelling tool for predicting survival of individual patients following resection of glioblastoma: A proof of principle. *British Journal of Cancer* **98**, 113–119. doi:10.1038/sj.bjc.6604125 (2008).
115. Swanson, K., Bridge, C., Murray, J. & Jr., E. A. Virtual and real brain tumors: Using mathematical modeling to quantify glioma growth and invasion. *Journal of the Neurological Sciences* **216**, 1–10. doi:10.1016/j.jns.2003.06.001 (2003).
116. Swanson, K. R. *et al.* Quantifying the role of angiogenesis in malignant progression of gliomas: in silico modeling integrates imaging and histology. *Cancer Research* **71**, 7366–7375. doi:10.1158/0008-5472.CAN-11-1399 (2011).
117. Syga, S., Jain, H. P., Krellner, M., Hatzikirou, H. & Deutsch, A. Evolution of phenotypic plasticity leads to tumor heterogeneity with implications for therapy. *PLOS Computational Biology* **20**, 1–18. doi:10.1371/journal.pcbi.1012003 (2024).
118. Tektonidis, M. *et al.* Identification of intrinsic in vitro cellular mechanisms for glioma invasion. *Journal of Theoretical Biology* **287**, 131–147. doi:10.1016/j.jtbi.2011.07.012 (2011).
119. Thiessen, R. & Hillen, T. Anisotropic network patterns in kinetic and diffusive chemotaxis models. *Mathematics* **9**, 1561. doi:10.3390/math9131561 (2021).
120. Turing, A. M. The chemical basis of morphogenesis. *Philosophical Transactions of the Royal Society of London. Series B, Biological Sciences* **237**, 37–72. doi:10.1098/rstb.1952.0012 (1952).

121. Tursynkozha, A., Kashkynbayev, A., Shupeyeva, B., Rutter, E. M. & Kuang, Y. Traveling wave speed and profile of a “go or grow” glioblastoma multiforme model. *Communications in Nonlinear Science and Numerical Simulation* **118**, 107008. doi:[10.1016/j.cnsns.2022.107008](https://doi.org/10.1016/j.cnsns.2022.107008) (2023).
122. Van der Stelt, S., Doelman, A., Hek, G. & Rademacher, J. D. M. Rise and fall of periodic patterns for a generalized Klausmeier–Gray–Scott model. *Journal of Nonlinear Science* **23**, 39–95. doi:[10.1007/s00332-012-9139-0](https://doi.org/10.1007/s00332-012-9139-0) (2013).
123. Venegas-Ortiz, J., Allen, R. J. & Evans, M. R. Speed of invasion of an expanding population by a horizontally transmitted trait. *Genetics* **196**, 497–507. doi:[10.1534/genetics.113.158642](https://doi.org/10.1534/genetics.113.158642) (2014).
124. Vittadello, S. T., McCue, S. W., Gunasingh, G., Haass, N. K. & Simpson, M. J. Examining go-or-grow using fluorescent cell-cycle indicators and cell-cycle-inhibiting drugs. *Biophysical Journal* **118**, 1243–1247. doi:[10.1016/j.bpj.2020.01.036](https://doi.org/10.1016/j.bpj.2020.01.036) (2020).
125. Wang, M. & Pang, P. Y. *Upper and lower solutions method for single equations in Nonlinear Second Order Elliptic Equations* 63–129 (Springer, 2024). doi:[10.1007/978-981-99-8692-7_3](https://doi.org/10.1007/978-981-99-8692-7_3).
126. Wang, S. D. *et al.* EphB2 receptor controls proliferation/migration dichotomy of glioblastoma by interacting with focal adhesion kinase. *Oncogene* **31**, 5132–5143. doi:[10.1038/onc.2012.16](https://doi.org/10.1038/onc.2012.16) (2012).
127. Wang, Y. & Shi, J. Analysis of a reaction-diffusion benthic-drift model with strong Allee effect growth. *Journal of Differential Equations* **269**, 7605–7642. doi:[10.1016/j.jde.2020.05.044](https://doi.org/10.1016/j.jde.2020.05.044) (2020).
128. Weinberger, H. F., Lewis, M. A. & Li, B. Analysis of linear determinacy for spread in cooperative models. *Journal of Mathematical Biology* **45**, 183–218. doi:[10.1007/s002850200145](https://doi.org/10.1007/s002850200145) (2002).
129. Wick, W., Osswald, M., Wick, A. & Winkler, F. Treatment of glioblastoma in adults. *Therapeutic Advances in Neurological Disorders* **11**, 1756286418790452. doi:[10.1177/1756286418790452](https://doi.org/10.1177/1756286418790452) (2018).
130. Xie, Q., Mittal, S. & Berens, M. E. Targeting adaptive glioblastoma: An overview of proliferation and invasion. *Neuro-oncology* **16**, 1575–1584. doi:[10.1093/neuonc/nou147](https://doi.org/10.1093/neuonc/nou147) (2014).
131. Xin, J. Front propagation in heterogeneous media. *SIAM Review* **42**. doi:[10.1137/S003614459936429](https://doi.org/10.1137/S003614459936429) (2000).
132. Yan, X., Nie, H. & Zhou, P. On a competition-diffusion-advection system from river ecology: Mathematical analysis and numerical study. *SIAM Journal on Applied Dynamical Systems* **21**, 438–469. doi:[10.1137/20M1387924](https://doi.org/10.1137/20M1387924) (2022).
133. Zhang, T. Minimal wave speed for a class of non-cooperative reaction–diffusion systems of three equations. *Journal of Differential Equations* **262**, 4724–4770. doi:[10.1016/j.jde.2016.12.017](https://doi.org/10.1016/j.jde.2016.12.017) (2017).
134. Zhang, T. & Wang, W. Existence of traveling wave solutions for influenza model with treatment. *Journal of Mathematical Analysis and Applications* **419**, 469–495. doi:[10.1016/j.jmaa.2014.04.068](https://doi.org/10.1016/j.jmaa.2014.04.068) (2014).

135. Zhang, T., Wang, W. & Wang, K. Minimal wave speed for a class of non-cooperative diffusion–reaction system. *Journal of Differential Equations* **260**, 2763–2791. doi:[10.1016/j.jde.2015.10.017](https://doi.org/10.1016/j.jde.2015.10.017) (2016). 1264
1265
1266
136. Zhao, X.-Q. & Zhou, P. On a Lotka–Volterra competition model: The effects of advection and spatial variation. *Calculus of Variations and Partial Differential Equations* **55**, 73. doi:[10.1007/s00526-016-1021-8](https://doi.org/10.1007/s00526-016-1021-8) (2016). 1267
1268
1269
137. Zhigun, A., Surulescu, C. & Hunt, A. A strongly degenerate diffusion-haptotaxis model of tumour invasion under the go-or-grow dichotomy hypothesis. *Mathematical Methods in the Applied Sciences* **41**, 2403–2428. doi:[10.1002/mma.4749](https://doi.org/10.1002/mma.4749) (2018). 1270
1271
1272
138. Zhu, H. & Ou, C. Existence of traveling wavefronts for Sherratt’s avascular tumor model. *Chaos, Solitons & Fractals* **44**, 218–225. doi:[10.1016/j.chaos.2011.01.011](https://doi.org/10.1016/j.chaos.2011.01.011) (2011). 1273
1274
1275
139. Zhu, H., Yuan, W. & Ou, C. Justification for wavefront propagation in a tumour growth model with contact inhibition. *Proceedings of the Royal Society A: Mathematical, Physical and Engineering Sciences* **464**, 1257–1273. doi:[10.1098/rspa.2007.0097](https://doi.org/10.1098/rspa.2007.0097) (2008). 1276
1277
1278